course of the study for reasons other than scrapie infection were not included in the final calculation of infectious titers. Infectious titers were expressed as a 50% lethal dose (LD_{50}) according to the method of Kärber [16].

Samples taken before and after filtration during the P-15N/antithrombin (AT; previously named antithrombin-III) study were tested for the presence of scrapie infectivity using a qualitative hamster bioassay. Syrian hamsters were inoculated with undiluted samples only, as described above, except that only three animals were used per sample.

2.5. Evaluation of PrP^{Sc} removal in the presence of plasma preparations

To investigate whether differences in how the scrapie spike material was prepared influenced our evaluation of prion removal, two different spiked preparations were compared using the manufacturing process for preparing AT (Neuart®, Benesis Corp., Osaka, Japan). Samples taken during the actual manufacturing process, immediately before the Planova step, were spiked with 263K MF treated with 0.1% (w/v) sarkosyl for 30 min at room temperature, or with 220 nm-filtered "super-sonicated" 263K MF. The spiked AT materials were then passed through a P-15N filter. The influence of different filtration conditions on the removal of PrP^{Sc} was compared for the same spike preparations, and for different spike preparations, using heat/PEG-treated intravenous immunoglobulin (IVIG) (Venoglobulin-IH, Benesis Corp.) and haptoglobin (Haptoglobin Injection-Yoshitomi, Benesis Corp.). Samples taken during the actual manufacturing process, immediately before the Planova step, were spiked with: 220 nm-filtered "super-sonicated" 263K MF (IVIG/P-35N and haptoglobin/P-35N); 263K MF ultracentrifuged at 141,000 × *g* for 60 min at 4 °C, resuspended in buffer equivalent to the starting material without protein, "super-sonicated" and 220 nm-filtered (IVIG/P-20N); or 263K MF treated with 0.3% (v/v) TNBP/1% (v/v) Tween 80 for 6 h at 30 °C ("SD treatment"), ultracentrifuged at 141,000 × *g* for 60 min at 4 °C, resuspended in saline, "super-sonicated", and 220 nm-filtered (haptoglobin/P-20N). The spiked material was then passed through either a P-35N filter or a P-20N filter (19 ± 2 nm). Although not part of the manufacturing process for haptoglobin, the SD treatment was included for the spiked preparation in an effort to reduce the clogging of the filter that occurs following the addition of a prion spike. Filtration processes for the thrombin preparation (Thrombin-Yoshitomi, Benesis Corp.) were also investigated. For thrombin, a sample taken during the actual manufacturing process immediately before the Planova step was spiked with 263K MF subjected to "SD treatment" followed by ultracentrifugation at 141,000 × *g* for 60 min at 4 °C, resuspended in the starting material, "super-sonicated" and 220 nm-filtered, and the spiked material then passed through a P-15N filter.

The experimental conditions used in the prion removal studies were designed to mimic the conditions used during the actual manufacturing process for the relevant product. For all processes, samples were analyzed by WB. The $\log_{10}$ reduction factor (LRF) for PrP^{Sc} was calculated for each filtration run, by comparing the total amount of PrP^{Sc} present in samples before and after filtration. All studies involving the use of WB1 and 2, and the quantitative bioassays, were performed in facilities in compliance with current GLP regulations. Studies involving the determination of average particle size in normal MF preparations, the use of WB3, and the qualitative bioassay, were performed as non-GLP studies.

3. Results

3.1. Influence of MF preparation method on particle size distribution

Ideally, to represent a "worst case" challenge for a filter, the smallest form of prion protein, or infectious agent, should be used. Studies to investigate the optimum method for preparing the prion spike material were therefore performed. In these studies, changes in the average particle size in normal MF were investigated, as 263K-infected brain material could not be handled within our facility. Although prion particles in MF derived from 263K-infected brain material were not investigated directly, we tried to optimize the design of our experiments by minimizing the size of particles in normal MF, as particle size may influence filtration performance (both with respect to filter blockage, and removal of PrP^{Sc}). The results are shown in Figs. 1 and 2.

Treatment of normal MF with sarkosyl or lysolecithin reduced the average size of particles to approximately 100 nm, when 0.1% or higher concentrations of the detergents were used. However, below that concentration, the particle size did not change significantly, with the exception of 0.01% lysolecithin which reduced the average particle size to approximately 300 nm (Fig. 1A,B). Treatment with Triton X-100 did not result in a significant change in particle size, even at 1% (Fig. 1C). Treatment with 0.3% TNBP or 1% Tween 80 alone was not able to reduce the particle size below 200 nm. However, when combined, one of the conditions generally used for viral inactivation ("SD treatment"), 0.3% TNBP and 1% Tween 80 reduced the average particle size to below 200 nm (Fig. 1D). These results suggest that the reduction in average particle size in normal MF depends on the choice of detergent(s), and the concentration and combination of detergent(s) used.

We also studied the effect of "super-sonication" on the particle size in normal MF. The results showed that "super-sonication" could reduce the average particle size to a very fine level in a short time, without the need to change the composition of the normal MF material (Fig. 2A). Since "super-sonication" is a temporary physical procedure, reversal of the particle size reduction may possibly occur. To exclude this possibility during the experiments, we conducted a stability study on the particle size in normal MF after "super-sonication". There was no significant change in the particle size up to 24 h after "super-sonication", with the size remaining at approximately 100 nm (Fig. 2B).

The results showed that the particle size of normal MF preparations could be reduced significantly by treatment

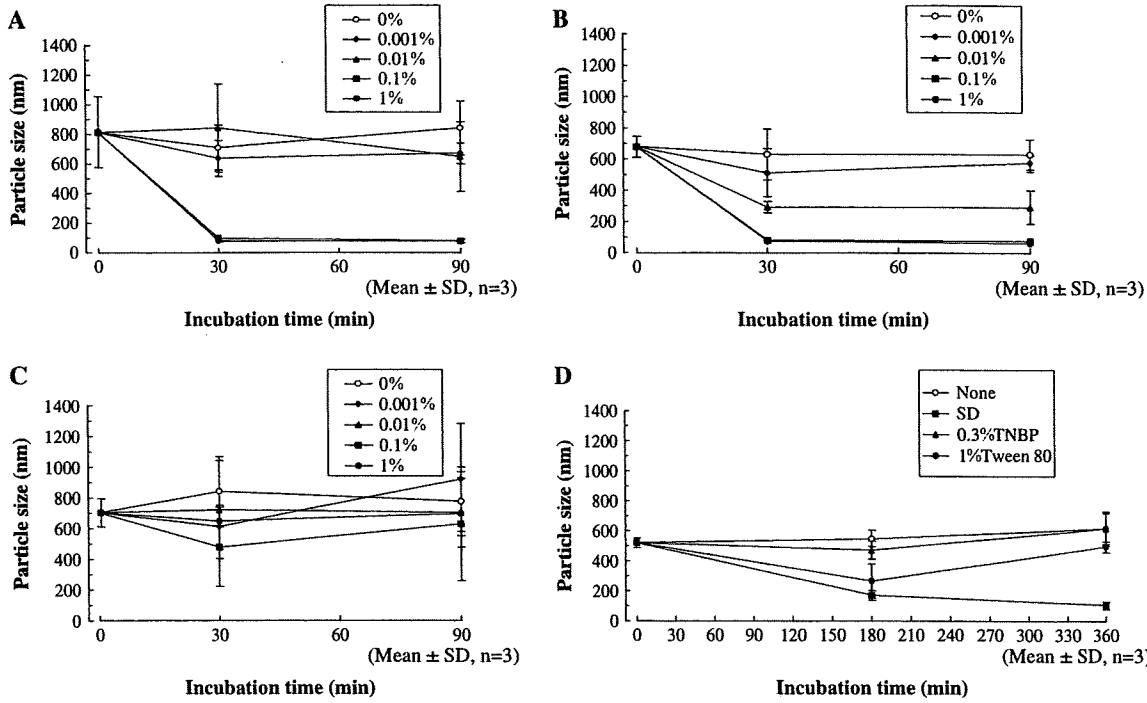

Fig. 1. Change of particle size in normal MF following treatment with various detergents. To normal MF, sarkosyl (A), lysolecithin (B), or Triton X-100 (C) was added to a final concentration of 1%, 0.1%, 0.01%, and 0.001%, respectively. The change in the average particle size was then monitored at room temperature for 90 min. In addition, TNBP or Tween 80 was added to normal MF to a final concentration of 0.3% and 1%, respectively, either alone, or in combination ("SD treatment"). The change in the average particle size was then monitored at 37 °C for 6 h (D).

with 0.1% sarkosyl, 0.1% lysolecithin, "SD treatment", or "super-sonication". The use of detergent or "SD treatment", in combination with "super-sonication", was also shown to effectively reduce the average particle size in normal MF preparations, to comparable levels to the individual treatments alone (data not shown). "Super-sonication" has an advantage over the other treatments in that it can minimize the change of composition of samples taken from the manufacturing process, as it does not require the addition of reagent(s) to the normal MF. For this reason, "super-sonication" is considered to be a useful approach for the treatment of 263K MF for process evaluation. "SD treatment", although slightly less effective, is used in many manufacturing processes, and may therefore be useful alone, or in combination with "super-sonication", for the process evaluation of products whose manufacturing process includes an "SD treatment" step. These approaches, alone or in combination, may also be useful to prevent the clogging of filters that can occur during spiking studies.

3.2. Infectivity of PrP^{Sc} in 263K MF and influence of 263K MF preparation methods on infectivity

The effect of "super-sonication" and "SD treatment" on the infectivity of 263K MF was studied. Infectious titers of

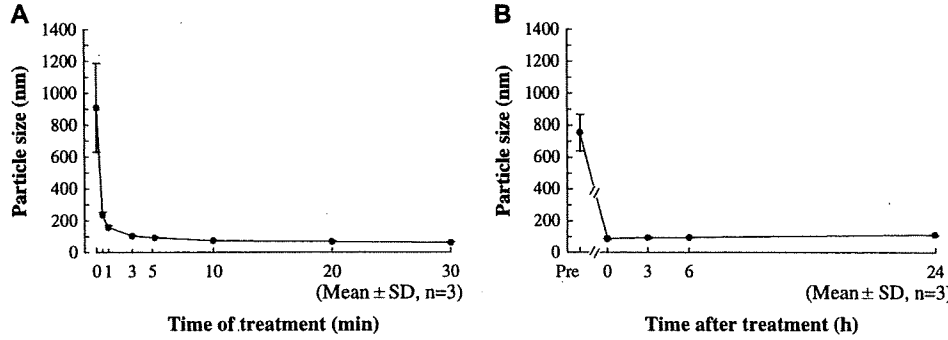

Fig. 2. Change of particle size in normal MF following intense sonication ("super-sonication"). Normal MF in a test tube equipped with a resonance chip (20 kHz, 200 W) was sonicated for 1 min in an ice bath. After 1 min, the sonication step was repeated. The change in average particle size was monitored during 30 cycles of sonication (A). After 10 cycles of sonication ("super-sonication"), normal MF was held at room temperature for 24 h, and the change in particle size was monitored (B).

263K MF, "super-sonicated" 263K MF, and 263K MF subjected to "SD treatment", ultracentrifuged at 141,000 × *g* for 60 min at 4 °C, resuspended with thrombin starting material, "super-sonicated", and 220 nm-filtered, were determined using a hamster bioassay. The results are summarized in Table 1.

The titers of two independent batches of 263K MF treated by "super-sonication" were 6.0 and 5.3 $\log_{10}$ LD_{50}/ml, respectively. The titer of the "non-super-sonicated"263K MF used to generate one of these stocks was 5.7 $\log_{10}$ LD_{50}/ml. These results suggest that "super-sonication" does not influence the infectivity of 263K MF. The titer of the 263K MF subjected to "SD treatment", ultracentrifuged at 141,000 × *g* for 60 min at 4 °C, resuspended with the thrombin starting material, "super-sonicated", and 220 nm-filtered, was 6.9 $\log_{10}$ LD_{50}/ml, which was approximately 1 log higher than that of the corresponding stock treated by "super-sonication" alone. Whether this difference is significant is unclear. The process to generate the "SD-treated" spike materials included an ultracentrifugation step. We were therefore concerned about recovery of infectivity following centrifugation, as the particle size of 263K MF was highly reduced by the "SD treatment" step. However, these results suggested that the recovery of infectious particles following ultracentrifugation was satisfactory.

Although it is possible that use of a 200 day bioassay may under-estimate the infectious titer of the 263K MF stocks, the use of a relatively short duration bioassay is considered unlikely to affect the main conclusions drawn. At least the last two dilution groups tested showed no animals with evidence of scrapie infection in all four titrations, and only three animals in the study (one in each of three separate titrations) developed clinical symptoms necessitating euthanasia later than day 131 (euthanized on days 160, 183 and 183, respectively), suggesting the titers obtained for all the stocks are close to end-point (data not shown). In addition, as others have demonstrated that treatment with detergent, and exposure to treatments that result in inactivation of the scrapie agent, such as heat or NaOH, may result in extended incubation periods for clinical scrapie, if anything the results may under-estimate the relative titers of the treated stocks [17,18]. Therefore, the bioassay results support the conclusion that "super-sonication" of 263K MF stocks, with or without "SD treatment", does not appear to significantly reduce the infectious titer of the stock, and that these preparations are therefore suitable for use in prion clearance studies.

3.3. Removal of PrP^{Sc} by various filters

To determine whether "super-sonication" influenced the $\log_{10}$ reduction observed for PrP^{Sc} following filtration under defined conditions, "super-sonicated" or "non-super-sonicated" stocks of 263K MF were diluted in PBS, and then filtered through 220 nm, 100 nm, P-75N, P-35N and P-15N filters. Samples were analyzed by WB. The results are summarized in Table 2. The use of "super-sonicated" 263K MF appeared to result in lower $\log_{10}$ reduction values, supporting the idea that "super-sonication" of 263K MF produces a more severe challenge for a filter step. An approximately 5-fold higher $\log_{10}$ reduction factor was observed for "non-super-sonicated" stocks, for the 100 nm and P-75N filters, for both stocks tested. No significant loss of PrP^{Sc} was observed with either spiking material with 220 nm filtration, and no PrP^{Sc} was detected in the filtrates following P-35N and P-15N filtration.

Previously, we have observed some removal of PrP^{Sc} in some lots of "non-super-sonicated" 263K MF by 220 nm filtration. Strict control of the methodology used to generate the 263K MF stocks appeared to prevent this, suggesting that the method of preparing the 263K MF itself may influence the particle size distribution (data not shown).

3.4. Removal of PrP^{Sc} by Planova filters in the presence of plasma preparations

Removal of PrP^{Sc} by P-15N, P-20N, and P-35N filters was evaluated in the presence of a number of different plasma preparations, under conditions designed to mimic the relevant manufacturing process. The design of the experiments was similar to that of virus clearance studies. Samples were analyzed by WB, and the $\log_{10}$ reduction factor (LRF) was calculated for each filter step. The results are shown in Table 3.

Under all the experimental conditions tested, PrP^{Sc} was not detected by WB after filtration through P-15N. The LRF values were $\geq$2.8. In contrast, PrP^{Sc} was detected by WB in samples following filtration through P-20N and P-35N filters, in three out of the four processes tested, giving LRF values in the order of 2 logs. In one study, P-35N/haptoglobin, using "super-sonicated" 263K MF, PrP^{Sc} was not detected in the filtrate. However, the sensitivity of this study was low, giving a LRF of $\geq$1.4, and therefore the robustness of this filtration process was not evaluated. In the initial studies (Table 2), PrP^{Sc} was not detected in the fractions after P-35N filtration of either "super-sonicated" or "non-super-sonicated" 263K MF in PBS, resulting in log reduction factors in the order of 3 logs. The variance in the results obtained for these filters could be due to a combination of factors, including how the scrapie spike material was prepared, the composition of the starting material, and the precise filtration conditions used.

3.5. Removal of prion infectivity by Planova filters in the presence of plasma preparations

P-15N filtration was shown in these studies to be able to remove PrP^{Sc} to levels below the detection limit of the WB assays used, regardless of the method used to prepare the spike material, the composition of the start material, or the filtration conditions. However, a bioassay study for samples generated in a P-15N/AT study using 220 nm-filtered "super-sonicated" 263K MF, demonstrated that infectivity was recovered following filtration, as clinical signs appeared in all hamsters inoculated with the filtrate, and analysis of hamster brain material confirmed the clinical results. PrP^{Sc} was detected in the brain homogenates from all clinically positive hamsters by WB, and scrapie-associated lesions were observed in all the

Table 4
Scrapie infectivity in samples generated during the P-15N/AT study

	Before filtration			Filtrate		
	Animal number			Animal number		
	1	2	3	1	2	3
Appearance of clinical signs (day euthanized)	87	87	87	94	143	105
PrP^{Sc} in brain by WB3	Detected	Detected	Detected	Detected	Detected	Detected
Lesions by histopathology	+ve	+ve	+ve	+ve	+ve	+ve
Medulla (oblongata)	D,V,P	D,V,P	D,V,P	D,V,P	D,V,P	D,V,P
Cerebellum (cortex)	D	D,V,P	D,V,P	D,V,P	D,V,P	D,V,P
Midbrain	D,P	D,V,P	V,P	D,P	D,P	D,V,P
Hypothalamus	D,P	D,V,P	D,P	D,V,P	D,P	D,P
Thalamus	D,P	D,V,P	D,P	D,P	D,P	D,P
Hippocampus	NR	D,V	D	D	D,V,P	D,V
Paraterminal body	D,P	D,P	D,P	NR	D,V,P	P
Cerebral cortex (posterior midline)	D,P	D,P	D,P	D,P	D,V,P	D,V,P
Cerebral cortex (anterior midline)	D,P	D,V,P	D,V,P	D,V,P	D,V,P	D,V,P

Abbreviations used: +ve, scrapie positive; NR, no remarkable change; D, degeneration of nerve cell; V, vacuolation; P, proliferation of glial cell.

corresponding hamster brain material on histopathological observation (Table 4). Typical nerve lesions are shown in Fig. 3. Thus, P-15N filtration did not result in the complete removal of infectivity, for this process step.

4. Discussion

In this study, we have investigated the capacity of P-35N, P-20N and P-15N filters to remove the 263K scrapie prion protein, PrP^{Sc}, under the conditions used for the manufacture of four different plasma-derived products, using spike preparations designed to present a serious challenge to the filters.

Validation studies to evaluate the capacity of manufacturing processes to remove potential contaminants, including prions, are required for biological or biopharmaceutical products intended for human use. When designing these studies, a worst-case challenge should be used wherever possible, to minimize the risk of over-estimating the capacity of the process to remove such contaminants. Virus removal filters (or nanofilters) are designed to remove contaminants predominantly on the basis of size. The worst-case challenge for such steps should therefore be a preparation containing the smallest possible form of the infectious agent.

TSE clearance studies provide a particular challenge in that the nature of the infectious agent is still uncertain, and the forms of infectious agent present in plasma, and/or during the different stages of a manufacturing process, are not clearly understood. The causative agent of TSE diseases is believed to be strongly associated with, if not solely composed of, the disease-associated prion protein, PrP^{Sc}. Normal cellular PrP is a membrane-bound glycoprotein, which associates with membranes through a glycosylphosphatidylinositol (GPI) anchor. Prion infectivity is associated with heterogeneous particles, including membranes, liposomes and protein aggregates, so called prion rods. Therefore, methods which result in solubilization of membrane proteins, or dispersal of membrane fragments, vesicles and/or protein aggregates, may be expected to reduce the size of particles associated with prion infectivity.

Treatment of MF preparations derived from brains of uninfected (normal) hamsters with either detergent (0.1% lysolecithin or 0.1% sarkosyl) or extensive sonication ("supersonication") resulted in a rapid reduction in the average particle size, to approximately 100 nm. SD treatment (1% Tween 80 and 0.3% TNBP for 6 h) also resulted in a reduction in particle size, although this was slower and less effective, reducing the average particle size to the order of 200 nm.

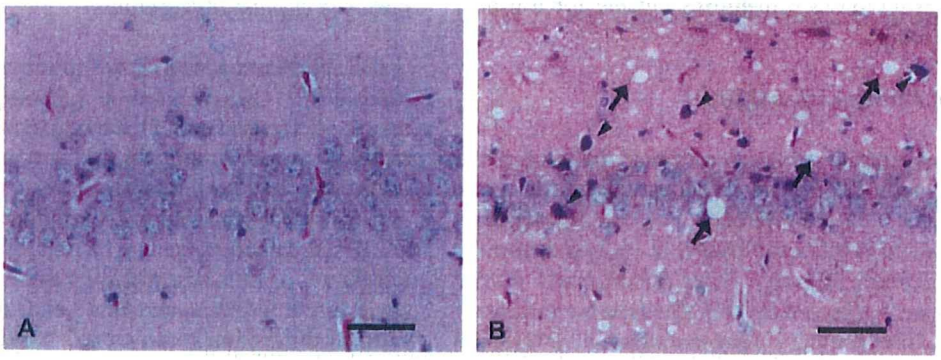

Fig. 3. Typical nerve lesions in the hippocampus of a hamster brain, taken from an animal inoculated with a P-15N-filtered sample (B), in comparison with the corresponding region from an uninfected animal (A). Arrows, vacuolation; Arrowheads, degeneration of nerve cells; scale bar = 50 μm; HE staining used.

"Super-sonication" has the advantage that it is a physical disruption process, and does not alter the chemical composition of the spike material, thus minimizing changes to the start material used for nanofiltration. SD treatment is included in many manufacturing processes for plasma-derived products, and therefore, although not as effective as "super-sonication", use of this treatment might be expected to result in a spike material more closely mimicking the form of infectious prion present in the relevant start material during the manufacturing process. Use of these treatments alone or in combination may therefore be useful in reducing the size of infectious particles present in TSE spike materials for prion clearance studies.

The effect of the above treatments was studied using normal MF, as the facility was unable to handle infectious TSE materials. Although some care should be taken in extrapolating these results to TSE-infected brain material, "super-sonication" of 263K MF preparations appeared to reduce the removal of PrP^{Sc} following filtration, while detergent-treated spike preparations have previously been shown to present a more significant challenge to nanofiltration steps than untreated preparations ([9,10] and own unpublished observations). Furthermore, "super-sonication", with or without SD treatment, does not appear to reduce the level of infectivity present within the 263K MF, supporting the use of such preparations for prion clearance studies.

Using 263K MF treated with 0.1% sarkosyl, "super-sonication" or SD plus "super-sonication", we investigated the prion removal capacity of P-15N, P-20N and P-35N filters in the manufacturing processes used for four different plasma products. The results obtained suggest that both the composition of the materials to be filtered and the prion load influences the removal of prions. PrP^{Sc} was recovered in the filtrate fraction from three out of the four processing steps performed for P-20N and P-35N. In contrast, under all conditions tested, P-15N filtration resulted in removal of PrP^{Sc} to below the limit of detection of the Western blot assays used. Thus, P-15N would appear to be a more robust method for the removal of prions, reproducibly giving LRF in the order of 3 logs, under the conditions tested. In practice, however, it is not feasible to incorporate P-15N filtration into the manufacturing process for all plasma derivatives. From the results shown in Table 2, it may also be possible to optimize processing conditions to allow effective removal of PrP^{Sc} using P-20N or P-35N filters.

WB assays were used to monitor the partitioning of PrP^{Sc} during the nanofiltration processes. WB assays are semi-quantitative and serve to provide an indication of the relative levels of PrP^{Sc} present in different samples. However, there are limitations to the sensitivity of available WB assays, and these assays provide only an indirect measure of infectivity. Therefore, to confirm that removal of PrP^{Sc} does reflect removal of infectivity, bioassays need to be performed.

Although PrP^{Sc} was not detected in any of the P-15N filtered samples by WB assay, infectivity was recovered in a filtrate fraction tested by bioassay for one process run. Foster also noted that infectivity was detected in a filtrate fraction after P-15N filtration ([8] reported as personal communication; data not shown). Thus, even with P-15N, depending on the processing conditions, there may be incomplete removal of prion contaminants.

Although infectivity was detected in the filtrate fraction from the one process step studied, longer and more variable incubation periods were observed in the animals inoculated with the filtrate sample (Table 4), suggesting a lower prion titer following filtration. However, it was not possible to estimate the relative levels of prion infectivity present in the input and filtrate samples, as no data was available to correlate incubation periods and prion titers for this study. Based on the titers typically observed for 263K MF stocks, the bioassay used could theoretically detect reductions in prion infectivity in the order of 4 logs for this process step. Detection of infectivity in the filtrate fraction by bioassay is therefore not necessarily incompatible with the WB results obtained (LRF $\geq$2.8 logs), and may simply reflect a difference in sensitivity between the two assays used.

As discussed above, uncertainties about the nature of the infectious agent in plasma, and during the manufacturing process, raise concerns about the design and interpretation of prion clearance studies. No single spike preparation is likely to contain all potential forms of the infectious agent. Infectivity is associated with membranes and protein aggregates. In addition, it has recently been shown that the GPI anchor is not required for infectivity, suggesting that endogenous proteolytic release of PrP^{Sc} from cell surfaces may also contribute to the spread of the infectious agent *in vivo* [19,20]. Whether significant levels of infectivity in human plasma are associated with GPI-anchorless prion protein is not yet clear. These different forms of infectivity, with different biophysical properties, could show different partitioning properties through the same manufacturing process [7]. Furthermore, different forms of the agent may differ in their level of infectivity. For example, it was recently reported that particles in the order of 17–27 nm appeared to have the highest relative level of infectivity, in comparison to levels of PrP^{Sc} [21]. Therefore, a better understanding of the nature and forms of the infectious agent is essential to allow the design of more accurate models for prion clearance studies, and a more confident evaluation of the safety of manufacturing processes with respect to potential TSE contamination.

In summary, we used methods intended to reduce the size of particles present within MF preparations in an effort to present a worst-case (smallest) prion challenge during nanofiltration. Using such preparations, P-15N filtration consistently reduced the level of PrP^{Sc} to below the limits of detection of the Western blot assays used, suggesting that this process step is effective for the removal of prions. However, data from a single process step studied suggested that infectivity could be recovered following P-15N filtration, and thus even P-15N filtration may not result in complete removal of prions, at least when used under some conditions.

Acknowledgements

A part of this study was presented at the Planova workshop 2003 and 2006 held by Asahi Kasei. Asahi Kasei Medical Co., Ltd. kindly gave us permission to publish the entire study on

Planova filters. Some of the data presented in this study has been summarized in a recent review [22].

References

[1] Health Protection Agency. Fourth case of variant CJD infection associated with blood transfusion. Press release, http://www.hpa.org.uk/hpa/news/articles/press_releases/2007/070118_vCJD.htm, 18 January, 2007.

[2] Castilla J, Saá P, Soto C. Detection of prions in blood. Nature medicine 2005;11(9):982–5.

[3] European Medicines Agency/The Committee for Medicinal Products for Human Use (CHMP)/Biotechnology Working Party. CHMP position statement on Creutzfeldt–Jakob disease and plasma-derived and urine-derived medicinal products. EMEA/CPMP/BWP/2879/02/rev 1. London, http://www.emea.europa.eu/pdfs/human/press/pos/287902rev1.pdf, 23 June, 2004.

[4] The European Agency for the Evaluation of Medicinal Products/The Committee for Medicinal Products for Human Use (CHMP)/Biotechnology Working Party. Guideline on the investigation of manufacturing processes for plasma-derived medicinal products with regard to vCJD risk. CPMP/BWP/5136/03 London, http://www.emea.europa.eu/pdfs/human/bwp/513603en.pdf, 21 October, 2004.

[5] Strengthening of quality and safety assurance of drugs and medical devices manufactured using components of human origin as raw materials. PFSB notification no.0209003 dated February 9, 2005; Japan: MHLW (in Japanese).

[6] Stenland CJ, Lee DC, Brown P, Petteway Jr SR, Rubenstein R. Partitioning of human and sheep forms of the pathogenic prion protein during the purification of therapeutic proteins from human plasma. Transfusion 2002;42(11):1497–500.

[7] Vey M, Baron H, Weimer T, Gröner A. Purity of spiking agent affects partitioning of prions in plasma protein purification. Biologicals 2002; 30(3):187–96.

[8] Foster PR. Removal of TSE agents from blood products. Vox Sang 2004; 87(S2):7–10.

[9] Tateishi J, Kitamoto T, Ishikawa G, Manabe S. Removal of causative agent of Creutzfeldt-Jakob disease (CJD) through membrane filtration method. Membrane 1993;18(6):357–62.

[10] Tateishi J, Kitamoto T, Mohri S, Satoh S, Sato T, Shepherd A, et al. Scrapie removal using Planova® virus removal filters. Biologicals 2001;29(1): 17–25.

[11] Van Holten WR, Autenrieth S, Boose JA, Hsieh WT, Dolan S. Removal of prion challenge from an immune globulin preparation by use of a size-exclusion filter. Transfusion 2002;42(8):999–1004.

[12] Kimberlin RH, Walker CA. Characteristics of a short incubation model of scrapie in the golden hamster. J Gen Virol 1977;34(2):295–304.

[13] Kascsak RJ, Rubenstein R, Merz PA, Tonna-DeMasi M, Fersko R, Carp RI, et al. Mouse polyclonal and monoclonal antibody to scrapie-associated fibril proteins. J Virol 1987;61(12):3688–93.

[14] Lee DC, Stenland CJ, Hartwell RC, Ford EK, Cai K, Miller JLC, et al. Monitoring plasma processing steps with a sensitive Western blot assay for the detection of prion protein. J Virol Methods 2000; 84(1):77–89.

[15] Fraser H, Dickinson AG. The sequential development of the brain lesions of scrapie in three strains of mice. J Comp Pathol 1968;78(3):301–11.

[16] Kärber J. Beitrag zur kollektiven Behandlung pharmakologischer Reihenversuche. Arch Exp Path Pharmak 1931;162:480–3.

[17] Somerville RA, Carp RI. Altered scrapie infectivity estimates by titration and incubation period in the presence of detergents. J Gen Virol 1983; 64(9):2045–50.

[18] Taylor DM, Fernie K. Exposure to autoclaving or sodium hydroxide extends the dose-response curve of the 263K strain of scrapie agent in hamsters. J Gen Virol 1996;77(4):811–3.

[19] Lewis PA, Properzi F, Prodromidou K, Clarke AR, Collinge J, Jackson GS. Removal of the glycosylphosphatidylinositol anchor from PrP^{Sc} by cathepsin D does not reduce prion infectivity. Biochem J 2006; 395:443–8.

[20] Trifilo MJ, Yajima T, Gu Y, Dalton N, Peterson KL, Race RE, et al. Prion-induced amyloid heart disease with high blood infectivity in transgenic mice. Science 2006;313(5783):94–7.

[21] Silveira RJ, Raymond JG, Hughson GA, Race ER, Sim LV, Hayes FS, et al. The most infectious prion protein particles. Nature 2005;437(7056): 257–61.

[22] Yunoki M, Urayama T, Ikuta K. Possible removal of prion agents from blood products during the manufacturing processes. Future Virol 2006; 1(5):659–74.

Available online at www.sciencedirect.com
ScienceDirect
ELSEVIER
Biochemical and Biophysical Research Communications 366 (2008) 244–249
BBRC
www.elsevier.com/locate/ybbrc

Instability of familial spongiform encephalopathy-related prion mutants

Yasuko Watanabe [a], Wakako Hiraoka [b], Yuhei Shimoyama [c], Motohiro Horiuchi [d], Mikinori Kuwabara [a], Osamu Inanami [a,*]

[a] *Laboratory of Radiation Biology, Graduate School of Veterinary Medicine, Hokkaido University, Sapporo 060-0818, Japan*
[b] *Laboratory of Biophysics, School of Science and Technology, Meiji University, Kawasaki 214-8571, Japan*
[c] *Soft-Matter Physics Laboratory, Graduate School of Emergent Science, Muroran Institute of Technology, Muroran 050-8585, Japan*
[d] *Laboratory of Prion Diseases, Graduate School of Veterinary Medicine, Hokkaido University, Sapporo 060-0818, Japan*

Received 2 November 2007
Available online 4 December 2007

Abstract

We examined the influence of D177N (D178N in humans) mutation on the conformational stability of the S2 region of moPrP^{C} with varying pHs by using the SDSL–ESR technique. The ESR spectrum of D177N at pH 7.5 was narrower than that of Y161R1, referred to as WT*. The ESR spectrum of D177N did not change when pH in the solution decreased to pH 4.0. Our results suggested that the disappearance of a salt bridge (D177–R163) induced the increase in the instability of S2 region. Moreover, the line shape of the ESR spectrum obtained from H176S neighboring the salt bridge linked to the S2 region was similar to D177N. These results indicate that the protonation of H176 is strongly associated with the stability of S2 region. These findings are important for understanding the mechanism by which the disruption of the salt bridge in the S2 region forms the pathogenic PrP^{Sc} structure in hereditary prion disease.

Keyword: Prion protein; SDSL; ESR; Salt bridge; pH-sensitivity; D178N; Conformational stability; Histidine residue; Familial spongiform encephalopathy; Conformational transition

Transmissible spongiform encephalopathys (TSEs), or prion diseases, are a group of fatal neurodegenerative disorders including Creutzfeldt–Jacob disease (CJD), Gerstmann–Sträusler–Scheinker (GSS) syndrome and fatal familial insomnia (FFI) in humans, scrapie in sheep and bovine spongiform encephalopathy in cattle [1]. Though the precise mechanism and parameters of the conversion from the normal cellular prion protein (PrP^{C}) to the abnormal (scrapie-like and β-sheet-rich) form of prion protein (PrP^{Sc}) is still unknown, the accumulation of PrP^{Sc} in endosomes, the main intracellular acidic organelles, indicates that the process of conversion from PrP^{C} to PrP^{Sc} requires physiological acidic pH conditions [2–4].

The inherited prion diseases associated with mutations in the prion protein (*PRNP*) gene coding for PrP fall into three major groups: CJD, GSS syndrome and FFI [5]. Despite their phenotypic differences, FFI and one familial type of CJD (CJD_{178}) are both linked to a single mutation of *PRNP* at codon 178 resulting in the substitution of asparagine for aspartic acid (D178N) [6]. NMR data have revealed that a residue of Asp 178 (D178) forms a salt bridge with Arg 164 (R164), which holds the β-sheet against Helix 2 [7]. Moreover, the Molecular dynamics (MD) simulations indicate that the electrostatic interaction between D178 and R164 plays an important role in the dynamic stability of PrP^{C} [8]. Thus, it was proposed that the neutralization of D178 at low pH removes interactions that inhibit a structural change at neutral pH. In addition, His 187 (H187) has also been reported to be involved into a pathogenic mutation associated with GSS syndrome (H187R), which implies a positively charged residue in position 187, analogous to H187 protonation [9,10]. A recent study suggested that the breaking of the salt bridge between Glu 195 and Arg 156 induced by the protonation of H187 at acidic pH was the key event underlying the

* Corresponding author. Fax: +81 11 706 7373.
E-mail address: inanami@vetmed.hokudai.ac.jp (O. Inanami).

0006-291X/$ - see front matter © 2007 Elsevier Inc. All rights reserved.
doi:10.1016/j.bbrc.2007.11.145

extension of the S2 region [11]. However, there is no experimental evidence that these amino acids are involved in the structure of PrP^C such as the high flexibility of the S2 region.

Recently, to obtain experimental information about the pH-induced conformational changes, we employed cysteine-scanning site-directed spin labeling (SDSL) combined with electron spin resonance spectroscopy (ESR) and analyzed the pH-induced mobility changes in one α-helix (Helix 1) and two β-sheets (Sheet 1 and Sheet 2) of mouse PrP^C ($moPrP^C$) [12,13]. Our experimental data clearly demonstrated the presence of three pH-sensitive sites in $moPrP^C$, i.e. (1) the N-terminal tertiary contact site of Helix 1 (H1), (2) the C-terminal end of H1 and (3) the Sheet 2 (S2) region [13]. At low pH, a study using MD simulation showed loosening of the tertiary structure, extension of the S2 region and gain of an extended secondary structure in the N-terminal region followed by a misfolded intermediate rich in a β-like structure and a trimetric representation of a PrP^{Sc} protofibril [14]. In addition, high resolution NMR also suggested that the residues at the C-terminal end of H1 and β-strand 2 were involved in the "starting point" of pH-induced unfolding and implicated in endosomic PrP^C to PrP^{Sc} conformational transition resulting in TSEs [15]. Therefore, elucidation of how the pH-induced local mobility change correlated with the mechanism of the extension of the S2 region should provide important clues regarding the molecular basis of prion diseases.

In the present study, we examined the influence of mutations, D177N (D178N in humans) and H186S (H187S in humans), on the conformational stability of the S2 region of $moPrP^C$ at various pHs. For this purpose, we employed the SDSL–ESR method, since SDSL–ESR has been proven to be a powerful tool to monitor the structure and dynamics of proteins, which are impossible to obtain by NMR and X-ray crystallographic methods [12,13,16]. In our SDSL–ESR technique, the nitroxide side chain (R1) derived from (1-oxyl-2,2,5,5-tetramethylpyrroline-3-methyl)methane thiosulfonate (MTSSL) was introduced into a Tyr 161 (Y161) residue substituted for a cysteine residue by site-directed mutagenesis (Fig. 1A).

Materials and methods

Materials. (1-Oxyl-2,2,5,5-tetramethylpyrroline-3-methyl)methane thiosulfonate (MTSSL) was purchased from Toronto Research Chemicals (ON, Canada). 2-[4-(2-Hydroxyethyl)-1-piperazinyl]ethanesulfonic acid (HEPES) and 2-morpholinoethanesulfonic acid, monohydrate (MES) were from Dojindo, Lab. (Kumamoto, Japan). The Protein Assay Lowry Kit was from Nacalai Tesque, Inc. (Kyoto, Japan). Other reagents were from Wako Pure Chemical, Co. (Tokyo, Japan).

Construction, expression, purification, and spin-labeling of recombinant $moPrP^C$ mutants. These experimental procedures were based on those described previously [12,13]. To study the influences of amino acid residues Asp 177 and His 186 on the conformational stability of the S2 region around Y161R1, two plasmids containing double mutations, Y161C/D177N and Y161C/H186S, were constructed using this Y161C mutant as a template (Fig. 1B). In addition, we also created a plasmid encoding Y161C/H176S, to explore the effect of the positive charge of His 176 neighboring the salt bridge, D177–R164, on the structural stability of the S2 region. All $moPrP^C$ mutants (Y161C, Y161C/D177N, Y161C/H186S, and Y161C/H176S) were generated by the PCR-based site-directed mutagenesis method and confirmed their change using a CEQ8800 automated sequencer (Beckman Coulter, Inc.). Fig. 1B shows the positions of α-carbons of D177, H186, H176 (yellow) and Y161R1 (red) on the 3D structure in the carboxy-terminal domain of $moPrP_{(121-231)}$ as reported by Riek et al. (Potein Data Bank entry 1AG2) [17]. The expression and purification of recombinant $moPrP^C$ mutants were carried out as described previously [12,13]. To label the $moPrP^C$ mutants with MTSSL, a 10-fold molar excess of MTSSL was added to each protein and incubated overnight in the dark at 4 °C. The free MTSSL was removed from the protein using a microdialyzer (Nippon Genetics).

ESR spectroscopy. Details of the ESR spectroscopy methods have been published elsewhere [12,13]. The pH change of the sample solution was carried out by dialysis of the sample against eight buffers with various pH conditions from 4.0 to 7.5: 10 mM acetate buffer (pH 4.0, pH 4.5, and pH 5.0), 10 mM MES buffer (pH 5.5, pH 6.0, and pH 6.5) and 10 mM HEPES buffer (pH 7.0 and pH 7.5). ESR spectra were recorded in a quartz flat cell (RST-DVT05; 50 mm × 4.7 mm × 0.3 mm, Radical Research) for spin-labeled samples of 20 μM $moPrP^C$ using a JEOL-RE X-band spectrometer (JEOL) with a cylindrical TE011 mode cavity (JEOL). All ESR spectra were obtained at 10 °C, controlled by a temperature controller (ES-DVT4, JEOL), under the following conditions: 5 mW incident microwave power, 100 kHz modulation frequency, 0.2 mT field modulation amplitude and 15 mT scan range. The $1/\delta H_0$ of the central component ($M_I = 0$; ^{14}N hyperfine) in the ESR spectrum of spin-labeled $moPrP^C$ was employed as a mobility parameter and was further analyzed using a Win-Rad Radical Analyzer System (Radical Research). To analyze the stability of the S2 region in $moPrP^C$ mutants, we further measured the intensities of immobile (Im) and mobile (M) nitroxide probes in the low field component ($M_I = +1$) in each ESR spectrum.

Results and discussion

pH-induced conformational changes of the S2 region in $moPrP^C$

Many studies have demonstrated the relationship between the conversion from PrP^C to PrP^{Sc} and the pH in intracellular acidic compartments such as endosomes [2–4]. In a previous study, we also analyzed the pH-induced conformational changes in $moPrP^C$ using SDSL–ESR and provided experimental evidence for three pH-sensitive sites in the C-terminal region of $moPrP^C$ [12,13]. In particular, the Y161 in the N-terminal side of S2 region was identified as one of the highly sensitive site for pH change [13]. To obtain further information on the pH-sensitivity of this site, we investigated the pH-induced mobility changes of Y161R1 under various pH conditions from 4.0 to 7.5. In the present experiments, Y161R1 ($moPrP^C$ containing a single spin label at site 161 with no additional mutations) was used for examination of the stability of the S2 region in $moPrP^C$ and was referred to as WT*. The ESR spectrum of WT* observed at pH 7.5 showed a line broadening signal due to a major immobile component (Im) with a minor mobile component (M) (Fig. 2A). When the pH in the solution decreased from 7.5 to 4.0, the intensity of the mobile component increased relatively. To obtain detailed information about pH sensitivity, we measured $1/\delta H_0$ in ESR spectrum under various pH conditions from 7.5 to 4.0. The values of $1/\delta H_0$ obtained from the ESR spectra at

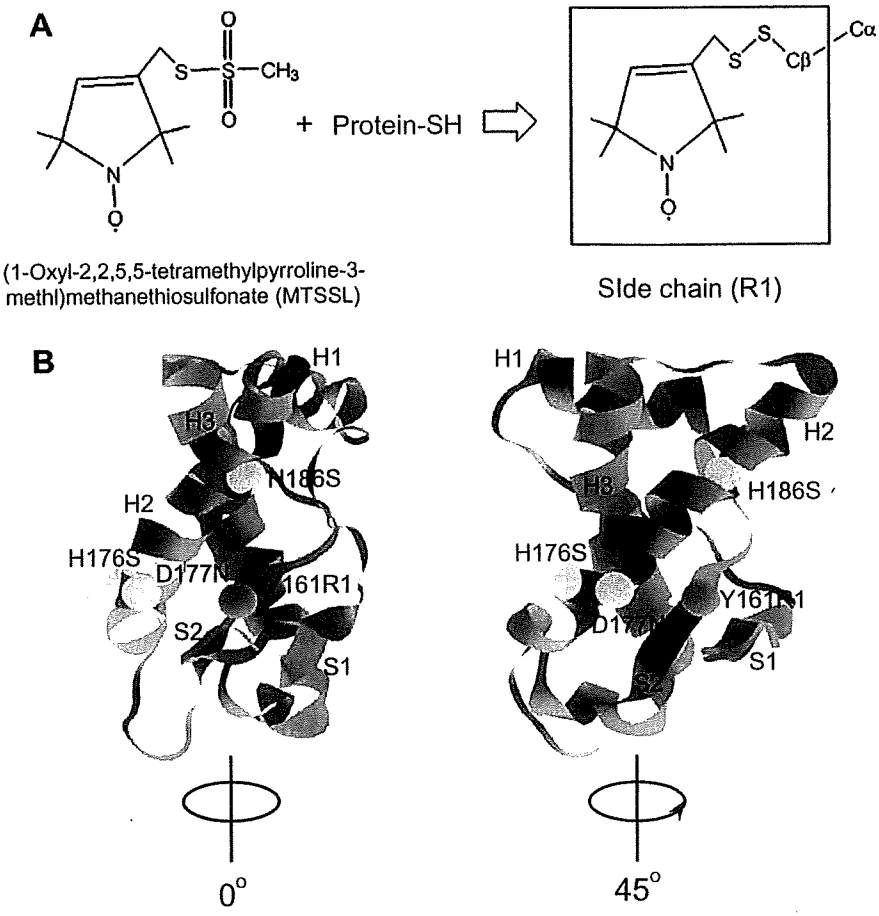

Fig. 1. A schematic diagram of the site-directed spin labeling (SDSL) technique and the mutation site for SDSL–ESR on the 3D structure of moPrP^{C}. (A) The reaction of the methanethiosulfonate spin-labeling reagent with the cysteine residue generates the nitroxide side chain (R1) on moPrP^{C}. (B) The carboxy-terminal domain of moPrP$_{(121-231)}$ and the mutation site for SDSL–ESR. Four α-carbons indicate the positions of D177, H186, H176 (yellow) and Y161R1 (red) in the pH-sensitive S2 region. These α-carbons were superimposed on the 3D structure of moPrP reported in an NMR study (PDB entry 1AG2, Ref. [17]). (For interpretation of color mentioned in this figure the reader is referred to the web version of the article.)

pH 7.5, pH 7.0, and pH 6.5 were approximately 1.66, 1.70, and 1.72, respectively, indicating that the nitroxide probes were strongly immobilized (Fig. 2B). In contrast, the $1/\delta H_0$ from the ESR spectra when the pH in the solution changed from 6.0 to 4.0 increased abruptly from approximately 1.84 to 2.11. These pH-dependent changes of $1/\delta H_0$ from ESR spectra were observed when the pH in the solution decreased to near pH 6.5 or less. Thus it was considered that the pH-dependent mobility change in the S2 region resulted in conformational transition.

Since the pH-dependent conformational change from a rigid to a flexible structure in the S2 region was clearly observed, we next examined whether isosbestic points were present in the ESR spectral changes induced by the decrease of pH. We prepared absorption spectra through integration of the first derivative spectrum in WT* at each pH from 7.5 to 4.0. In the superimposed spectra, six points that did not change during pH change were observed (Fig. 3C, black arrows). This observation indicated the presence of isosbestic points, suggesting that the conformational transition from a mobile structure to an immobile structure in the S2 region occurred at around pH 6.5. These findings indicated that the conformational transition occurred at between pH 6.5 and pH 6.0. These observations are the first evidence for structural instability in the S2 region in response to pH, which was assumed based on MD simulations [14].

Influence of the pathogenic mutations on the conformational stability of the S2 region with varying pH

Recently, MD simulation has shown that the mutation of Asp to Asn at position 178 plays an important role in the conformational conversion to β-sheet-rich PrP [18]. Linkages between familial prion diseases and mutations in the gene encoding human prion protein were reported and over 20 such mutations have been shown to date to segregate familial CJD, GSS and FFI [1,19,20]. The D178N mutation is one of the most intriguing disease-related mutations and leads to different phenotypes of human prion disease depending upon the polymorphism at position 129. The D178N mutant with methionine at 129 is associated with FFI, whereas the same mutant with valine at 129 correlates with hereditary CJD [6]. It was

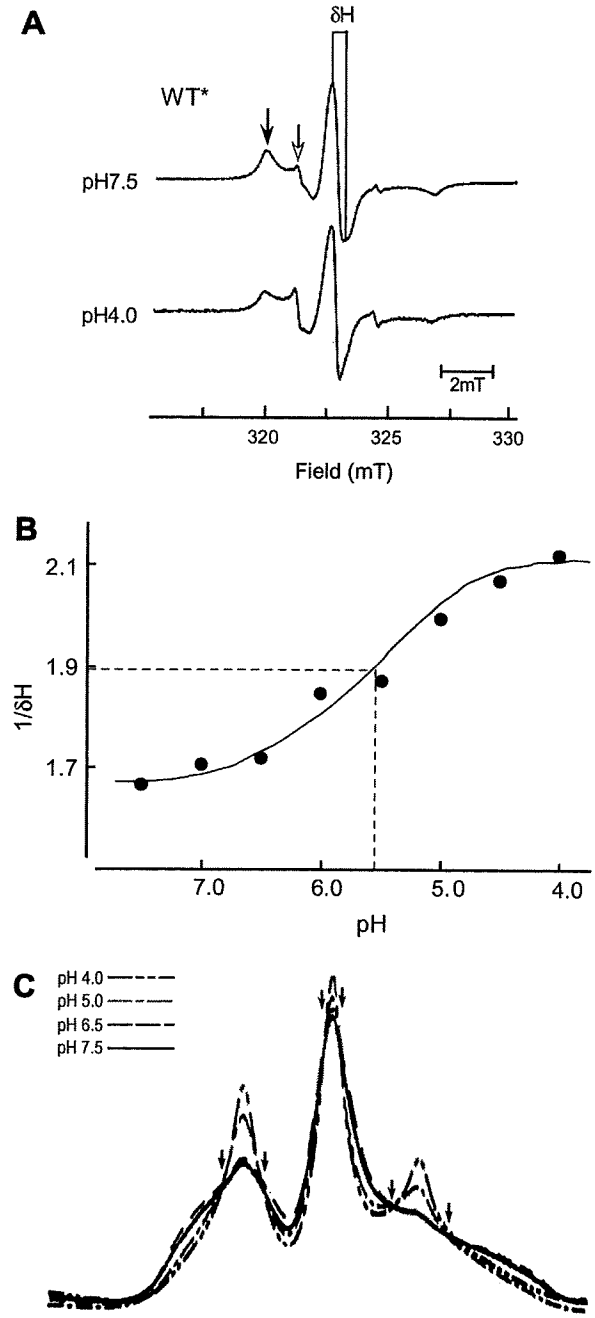

Fig. 2. The effect of pH on the ESR-spectra from the WT* mutant. (A) ESR spectra obtained from the WT* mutant at pH 7.5 and pH 4.0 were recorded using an X-band ESR spectrometer at 10 °C. The ESR spectrum at pH 7.5 showed a line broadening signal due to a major immobile component (Im, black arrow in $M_I = +1$) with a minor mobile component (M, white arrow in $M_I = +1$). (B) The changes of $1/\delta H_0$ from ESR spectra at various pHs from 7.5 to 4.0. The value of 1/δH obtained from the peak-to-peak central component ($M_I = 0$) in each ESR is plotted. It is considered that the pH-dependent mobility change in the S2 region results in conformational transition. (C) The absorption spectra obtained by integration of first derivative spectra in WT* at pH 7.5 (black line), pH 6.5 (blue line), pH 5.0 (violet line) and pH 4.0 (red line) are superimposed. Six black arrows show the isosbestic points that did not change during pH change. (For interpretation of color mentioned in this figure the reader is referred to the web version of the article.)

reported that the D178 side chain is involved in a salt bridge with R164, connecting Helix 2 with the β-sheet [8,21]. These reports led us to speculate that the D178N mutation induces a flexible structure of Helix 2 and the β-sheet by disruption of a salt bridge with R164. To clarify whether the mutations of D177 (D178 in humans) were actually associated with pH-dependent conformational changes in the S2 region, we measured the effects of pH changes on ESR spectrum of D177N. The ESR spectrum of D177N at pH 7.5 was narrower than that of WT* (Fig. 3A). The ESR spectrum of D177N did not change when the pH in the solution decreased from 7.5 to 4.0. Fig. 3B shows a summary of the stability of the S2 region in all mutants. We measured the intensities of immobile (Im) and mobile (M) nitroxide probes in the low field component ($M_I = +1$) and calculated the Im/M ratios at pH 7.5 and pH 4.0 for each ESR signal. At pH 7.5, the Im/M ratios of WT* were approximately 1.39. However, when the pH in the solution changed from 7.5 to 4.0, the Im/M ratios of WT* significantly decreased to 0.50. On the other hand, the Im/M ratios of D177N at pH 7.5 were approximately 0.39, significantly lower than that of WT*. Moreover, pH-dependent changes in the Im/M ratio were not observed for D177N. These results suggested that the structure around S2 of the PrP^C mutant with disappearance of this salt bridge was a flexible conformation, which was similar to that of WT* in the acidic condition. If the exposure of PrP^C to acidic conditions in endosomes is accepted as a key factor in the conversion to PrP^{Sc}, the unusual flexible structure of S2 of the D177N mutant at neutral pH may induce instability prone to pathogenic conversion.

Previous experiments using ^{2}H-NMR spectroscopy have shown that the pK_a values of glutamic acid at 22 and asparagic acid at 23 on $A\beta_{(1-40)}$ amyloid peptide are approximately 4.2–4.3, whereas the pK_a values of histidine at 13 and histidine at 14 are approximately 6.2 [22]. Analysis of Cu, Zn-superoxide dismutase showed that the pK_a value of the C-terminal histidine was 6.73 [23]. Since our data showed the conformational transition of WT* started from pH 6.5 (Fig. 2B and C), which was close to the pK_a of the histidine residue but not that of the asparagic acid residue, and the salt bridge (D177–R163) was essential for this pH-induced conformational transition in the S2 region of WT* as mentioned above, the histidine residue neighboring at the S2 region appeared to interfere with the interaction in the salt bridge (D177–R163). Therefore, we selected His 176 neighboring salt bridge D177–R163 and measured the ESR spectra of the H176S mutant. The line shape of the ESR spectrum obtained from H176S at pH 7.5 was narrower than that of WT* and the spectral change of H176S was small, when the pH in the solution decreased from 7.5 to 4.0 (Fig. 3A). The behavior of pH-dependent-spectral changes of H176S seemed to be close to that of D177N, rather than those of WT*, as indicated by the Im/M ratio (Fig. 3B). These results indicated that the H176 was strongly associated with the stability of S2 regions, although this histidine residue (human 177) was reported to have little effect on the overall spatial arrangement of PrP in an MD simulation study [11].

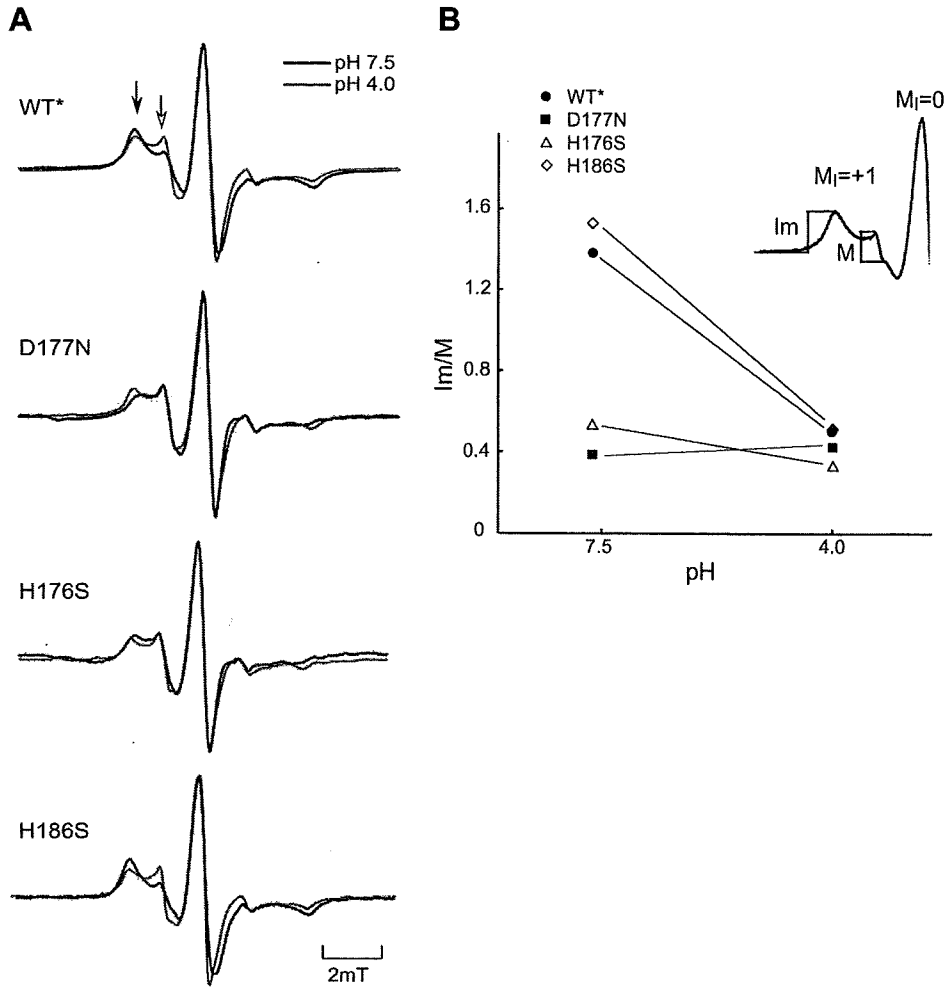

Fig. 3. The roles of amino acid residues D177, H176, and H186, in the pH-dependent conformational changes in the S2 region. (A) The ESR spectra of the WT*, D177N, H186S, and H176S mutants were obtained at pH 7.5 and pH 4.0. The line shapes of spectra were obtained at pH 7.5 (black line) and pH 4.0 (red line). The immobile component and mobile component are indicated by the black arrow and white arrow in the low field component ($M_I = +1$), respectively. (B) The stability of the S2 region in each moPrP^C mutants. The intensities of immobile and mobile nitroxide probes obtained from ESR spectra were measured and the ratios of Im/M were calculated. (For interpretation of color mentioned in this figure the reader is referred to the web version of the article.)

His 187 is reported to be involved in a pathogenic mutation associated with GSS syndrome (H187R) [9,10]. A recent study indicated that the breaking of the salt bridge (E195–R156) induced by the protonation of H187 at acidic pH was the key event underlying the extension of the S2 region [11]. However, in the present study, there were no differences in either the line shapes or the value of $1/\delta H_0$ from the ESR spectra of WT* and H186S at pH 7.5 (Fig. 3A). Furthermore, the ESR spectrum of H186S became narrower when pH was decreased from 7.5 to 4.0. This pH-dependent change in the line shape and Im/M ratio of H186S was quite similar to that of WT* (Fig. 3A and B). These result indicated that H186 was not involved in the pH-dependent instability in the S2 region. In humans, the trigger of pH-dependent conformational changes of GSS syndrome (H187R) may be different from those of FFI and CJD_{178} with point mutation of D178. Furthermore, we examined the conformational stability of the S2 region in the Q167R mutant, which acts as a dominant-negative, an inhibitory mutant against PrP^{Sc} formation (neighboring the S2 region) [24]. The pH-dependent mobility change in Q168R was also similar to WT* and H186S (data not shown). These results indicated that the conversion from PrP^C to PrP^{Sc} may be affected by several mechanisms of conformational change, including pH-dependent instability in the S2 region.

In conclusion, the present cysteine-scanning SDSL–ESR study for full-length recombinant moPrP^C provided experimental evidence that amino acid residues D177 and H176, but not H186, were important in the pH-induced conformational instability of the S2 region. In the D177N mutant, the mobility of the S2 region at natural pH was significantly higher than that in WT* and was similar to that in WT* at acidic pH. Moreover, the conformational transition of the S2 region started from pH 6.5, which was close to the pK_a of the histidine residue and the protonation of

H176 was strongly associated with the stability of S2 regions. These findings appear to be essential for understanding the mechanism by which the disruption of the salt bridge in the S2 region forms the pathogenic PrP^{Sc} structure in hereditary prion diseases.

Acknowledgments

We thank H. Tamayama and Y. Otoshima for ESR spectroscopy. This work was supported, in part, by Grants-in-Aid for Basic Scientific Research from the Ministry of Education, Culture, Sports, Science, and Technology of Japan (No. 17380178 and No. 18658118 [O.I.] and No. 17580275 and No. 17658126 [M.K.]), by Research Grants from the Program for the Center of Excellence of Zoonosis Control, Sapporo 060-0818, Japan [Y.W., O.I., M.H.] and CREST-JST, Multi-Quantum Coherence ESR Project, Muroran 050-8585, Japan [Y.S.].

References

[1] S.B. Prusiner, Prions, Proc. Natl. Acad. Sci. USA 95 (1998) 13363–13383.
[2] S. Hornemann, R. Glockshuber, A scrapie-like unfolding intermediate of the prion protein domain PrP(121–231) induced by acidic pH, Proc. Natl. Acad. Sci. USA 95 (1998) 6010–6014.
[3] W.-Q. Zou, N.R. Cashman, Acidic pH and detergents enhance *in vitro* conversion of human, brain PrP^{C} to a PrP^{Sc}-like form, J. Biol. Chem. 277 (2002) 43942–43947.
[4] D.A. Kocisko, S.A. Priola, G.J. Raymond, B. Chesebro, P.T. Lansbury Jr., B. Caughey, Species specificity in the cell-free conversion of prion protein to protease-resistant forms: a model for the scrapie species barrier, Proc. Natl. Acad. Sci. USA 92 (1995) 3923–3927.
[5] P. Parchi, P. Gambetti, Human prion diseases, Curr. Opin. Neurol. 8 (1995) 286–293.
[6] L.G. Goldfarb, R.B. Petersen, M. Tabaton, P. Brown, A.C. LeBlanc, P. Montagna, P. Cortelli, J. Julien, C. Vital, W.W. Pendelbury, M. Haltia, P.R. Wills, J.J. Hauw, P.E. McKeever, L. Monari, B. Schrank, G.D. Swergold, L. Autilio-Gambetti, D.C. Gajdusek, E. Lugaresi, P. Gambetti, Fatal familial insomnia and familial Creutzfeldt–Jakob disease: disease phenotype determined by a DNA polymorphism, Science 258 (1992) 806–808.
[7] R. Riek, G. Wider, M. Billeter, S. Hornemann, R. Glockshuber, K. Wüthrich, Prion protein NMR structure and familial human spongiform encephalopathies, Proc. Natl. Acad. Sci. USA 95 (1998) 11667–11672.
[8] J. Zuegg, J.E. Gready, Molecular dynamics simulations of human prion protein: importance of correct treatment of electrostatic interactions, Biochemistry 38 (1999) 13862–13876.
[9] L. Cervenakova, C. Buetefisch, H.S. Lee, I. Taller, G. Stone, C.J. Gibbs Jr., P. Brown, M. Hallett, L.G. Goldfarb, Novel *PRNP* sequence variant associated with familial encephalopathy, Am. J. Med. Genet. 88 (1999) 653–656.
[10] C.M. Bütefisch, P. Gambetti, L. Cervenakova, K.-Y. Park, M. Hallett, L.G. Goldfarb, Inherited prion encephalopathy associated with the novel *PRNP* H187R mutation, Neurology 55 (2000) 517–522.
[11] E. Langella, R. Improta, V. Barone, Checking the pH-induced conformational transition of prion protein by molecular dynamics simulations: effect of protonation of histidine residues, Biophys. J. 87 (2004) 3623–3632.
[12] O. Inanami, S. Hashida, D. Iizuka, M. Horiuchi, W. Hiraoka, Y. Shimoyama, H. Nakamura, F. Inagaki, M. Kuwabara, Conformational change in full-length mouse prion: a site-directed spin-labeling study, Biochem. Biophys. Res. Commun. 335 (2005) 785–792.
[13] Y. Watanabe, O. Inanami, M. Horiuchi, W. Hiraoka, Y. Shimoyama, F. Inagaki, M. Kuwabara, Identification of pH-sensitive regions in the mouse prion by the cysteine-scanning spin-labeling ESR technique, Biochem. Biophys. Res. Commun. 350 (2006) 549–556.
[14] M.L. DeMarco, V. Daggett, Local environmental effects on the structure of the prion protein, C.R. Biol. 28 (2005) 847–862.
[15] L. Calzolai, R. Zahn, Influence of pH on NMR structure and stability of the human prion protein globular domain, J. Biol. Chem. 278 (2003) 35592–35596.
[16] W.L. Hubbell, H.S. Mchaourab, C. Altenbach, M.A. Lietzow, Watching proteins move using site-directed spin labeling, Structure 4 (1996) 779–783.
[17] R. Riek, S. Hornemann, G. Wider, M. Billeter, R. Glockshuber, K. Wüthrich, NMR structure of the mouse prion protein domain PrP(121-321), Nature 382 (1996) 180–182.
[18] A.C. Apetri, D.L. Vanik, W.K. Surewicz, Polymorphism at residue 129 modulates the conformational conversion of the D178N variant of human prion protein 90–231, Biochemistry 44 (2005) 15880–15888.
[19] P. Gambetti, Q. Kong, W. Zou, P. Parchi, S.G. Chen, Sporadic and familial CJD: classification and characterization, Br. Med. Bull. 66 (2003) 213–239.
[20] J. Collinge, Prion diseases of humans and animals: Their causes and molecular basis, Annu. Rev. Neurosci. 24 (2001) 519–550.
[21] J. Gsponer, P. Ferrara, A. Caflisch, Flexibility of the murine prion protein and its Asp178Asn mutant investigated by molecular dynamics simulations, J. Mol. Graph. Model 20 (2001) 169–182.
[22] Z. Zhang, J.P. Lee, Selectively ^{2}H-labeled Glu/Asp: application to p*K*a measurements in Aβ amyloid peptide, J. Peptide Res. 55 (2000) 1–6.
[23] A. Myari, G. Malandrinos, Y. Deligiannakis, J.C. Plakatouras, N. Hadjiliadis, Z. Nagy, I. Sovago, Interaction of Cu(2+) with His-Val-His and of Zn(2+) with His-Val-Gly-Asp, two peptides surrounding metal ions in Cu,Zn-superoxide dismutase enzyme, J. Inorg. Biochem. 85 (2001) 253–261.
[24] V. Perrier, K. Kaneko, J. Safar, J. Vergara, P. Tremblay, S.J. DeArmond, F.E. Cohen, S.B. Prusiner, A.C. Wallace, Dominant-negative inhibition of prion replication in transgenic mice, Proc. Natl. Acad. Sci. USA 99 (2002) 13079–13084.

Journal of General Virology (2008), 89, 1533–1544 DOI 10.1099/vir.0.83578-0

Effect of intraventricular infusion of anti-prion protein monoclonal antibodies on disease progression in prion-infected mice

Chang-Hyun Song,[1] Hidefumi Furuoka,[2] Chan-Lan Kim,[1]† Michiko Ogino,[1]‡ Akio Suzuki,[1] Rie Hasebe[1] and Motohiro Horiuchi[1]

Correspondence
Motohiro Horiuchi
horiuchi@vetmed.hokudai.ac.jp

[1]Laboratory of Prion Diseases, Graduate School of Veterinary Medicine, Hokkaido University, Kita 18, Nishi 9, Kita-ku, Sapporo 060-0818, Japan

[2]Department of Pathobiological Science, Obihiro University of Agriculture and Veterinary Medicine, Inada-cho, Obihiro 080-8555, Japan

It is well known that anti-prion protein (PrP) monoclonal antibodies (mAbs) inhibit abnormal isoform PrP (PrP^{Sc}) formation in cell culture. Additionally, passive immunization of anti-PrP mAbs protects the animals from prion infection via peripheral challenge when mAbs are administered simultaneously or soon after prion inoculation. Thus, anti-PrP mAbs are candidates for the treatment of prion diseases. However, the effects of mAbs on disease progression in the middle and late stages of the disease remain unclear. This study carried out intraventricular infusion of mAbs into prion-infected mice before and after clinical onset to assess their ability to delay disease progression. A 4-week infusion of anti-PrP mAbs initiated at 120 days post-inoculation (p.i.), which is just after clinical onset, reduced PrP^{Sc} levels to 70–80 % of those found in mice treated with a negative-control mAb. Spongiform changes, microglial activation and astrogliosis in the hippocampus and thalamus appeared milder in mice treated with anti-PrP mAbs than in those treated with a negative-control mAb. Treatment with anti-PrP mAb prolonged the survival of mice infected with Chandler or Obihiro strain when infusion was initiated at 60 days p.i., at which point PrP^{Sc} is detectable in the brain. In contrast, infusion initiated after clinical onset prolonged the survival time by about 8 % only in mice infected with the Chandler strain. Although the effects on survival varied for different prion strains, the anti-PrP mAb could partly prevent disease progression, even after clinical onset, suggesting immunotherapy as a candidate for treatment of prion diseases.

Received 9 November 2007
Accepted 28 February 2008

INTRODUCTION

Prion diseases, such as scrapie, bovine spongiform encephalopathy (BSE) and Creutzfeldt–Jakob disease (CJD), are fatal neurodegenerative disorders characterized by accumulation of a disease-specific, abnormal isoform of the prion protein (PrP^{Sc}) in the central nervous system (CNS), astrogliosis, neuronal vacuolation and neuronal cell death. The appearance of BSE and variant CJD (vCJD), possibly linked to consumption of food derived from BSE-infected cattle, has increased awareness of prion diseases, but at present there is no effective treatment available for prion diseases. Given that transformation of a normal prion protein (PrP^{C}) to PrP^{Sc} is a central event in the pathogenesis of prion disease, compounds and/or strategies that inhibit PrP^{Sc} formation are of therapeutic interest.

Many compounds or strategies have been reported to inhibit PrP^{Sc} formation, including polyanions, glycosaminoglycans, phosphorothioate oligonucleotides, tetrapyrroles, polyene antibiotics, tricyclic compounds, PrP peptides, dominant-negative PrP, cysteine protease inhibitors, PrP immunization and small interfering RNAs (reviewed by Trevitt & Collinge, 2006). Most of these compounds and treatments antagonize PrP^{Sc} formation in cells persistently infected with prions. However, the anti-prion effects *in vivo* are not always consistent with those observed *in vitro*. Indeed, some of the compounds and treatments protect animals from experimental inoculation with prions or delay the onset of disease when administered before, simultaneously or soon after inoculation with prions via a peripheral route (Ehlers & Diringer, 1984; Farquhar & Dickinson, 1986; Ladogana *et al.*, 1992; Priola

†Present address: Foreign Animal Disease Division, Animal Disease Control Department, National Veterinary Research and Quarantine Service, 480 Anyang-6 dong, Manan-gu, Anyang 430-824, Republic of Korea.

‡Present address: Institute of Tropical Medicine, Nagasaki University, 1-12-4 Sakamoto, Nagasaki 852-8523, Japan.

et al., 2000). In addition, only a few compounds, such as amphotericin B, its derivative, MS-8209 and pentosan polysulfate (PPS), can prolong survival of mice infected with prions even when administered in the middle or late stage of prion infection via intracerebral inoculation (Demaimay *et al.*, 1997; Doh-ura *et al.*, 2004). Because intraventricular infusion of PPS at a late stage prolongs the incubation period of the disease in transgenic mice that overexpress PrP (Doh-ura *et al.*, 2004), clinical trials using PPS to treat human prion diseases are moving forward (Todd *et al.*, 2005). The current evidence suggests that PPS treatment of vCJD patients appears to have some beneficial effects, although the specificity of the effects still needs to be evaluated carefully (Rainov *et al.*, 2007).

Anti-PrP antibodies prevent direct interaction between PrP^{C} and PrP^{Sc} in a cell-free conversion reaction (Kaneko *et al.*, 1995; Horiuchi & Caughey, 1999). Subsequent reports have shown that anti-PrP antibodies prevent prion propagation in cells persistently infected with prion (Enari *et al.*, 2001; Peretz *et al.*, 2001; Gilch *et al.*, 2003; Kim *et al.*, 2004b; Perrier *et al.*, 2004; Feraudet *et al.*, 2005). The inhibitory effect of anti-PrP antibodies has also been demonstrated *in vivo*. Transgenic mice expressing monoclonal antibody (mAb) 6H4 were shown to be resistant to prion infection via the intraperitoneal route (Heppner *et al.*, 2001). Moreover, active immunization with recombinant PrP, synthetic PrP peptide or a DNA vaccine has been shown to delay the onset of the disease in mice following peripheral prion infection, although immunization was a prerequisite to obtain the prophylactic effect (Sigurdsson *et al.*, 2002; Schwarz *et al.*, 2003; Goñi *et al.*, 2005; Fernandez-Borges *et al.*, 2006). Passive immunization with anti-PrP antibodies was found to be effective in preventing prion infection via the peripheral route if antibodies were administered shortly after prion inoculation, but was not following intracerebral prion infection or if administered on or after clinical onset following intraperitoneal prion infection (White *et al.*, 2003). These results suggest that anti-PrP antibodies can protect against establishment of prion infection in peripheral tissues and thus may be useful for post-exposure prophylaxis. However, the therapeutic potential of anti-PrP antibodies, including whether or not anti-PrP antibodies antagonize prion propagation in the brain and can inhibit disease progression when applied after clinical onset, remains to be elucidated.

To evaluate the therapeutic effects of anti-PrP antibodies on prion diseases more precisely, we carried out intraventricular infusion of anti-PrP mAbs in mice that had been inoculated intracerebrally with prions. Here, we show that intraventricular infusion of anti-PrP mAbs reduced the level of accumulation of PrP^{Sc} and reduced spongiform changes and gliosis relative to negative controls. Furthermore, we observed prolongation of the incubation time in mice infected with the Chandler strain, even when infusion was initiated at the time of clinical onset of the disease.

METHODS

Antibodies. The following anti-PrP mAbs were used in this study: 106 (IgG2b), 110 (IgG2b), 31C6 (IgG1) and 44B1 (IgG2a). The mAbs 106, 110 and 31C6 recognized linear epitopes consisting of mouse PrP aa 88–90, 83–89 and 143–149, respectively, whereas mAb 44B1 recognized a discontinuous epitope within aa 155–231 (Kim *et al.*, 2004a). Anti-feline parvovirus mAb P2-284 (IgG1) was used as a negative control (Horiuchi *et al.*, 1997). The mAbs were dialysed for 3 days against PBS prior to intraventricular infusion. An Alexa Fluor 488 Protein Labelling kit (Molecular Probes) was used for fluorescent labelling of mAbs.

The following rabbit polyclonal antibodies were used as primary antibodies for immunohistochemistry: B103, which recognizes bovine PrP synthetic peptide aa 103–121 (Horiuchi *et al.*, 1995), anti-glial fibrillary acidic protein (GFAP; Dako) to visualize astrocytes and anti-Iba1 (Wako) to visualize microglia.

Mice and prion strains. All procedures for animal experiments were carried out according to protocols approved by the Institutional Committee for Animal Experiments. Mouse-adapted scrapie strains Obihiro and Chandler were used in this study. For intracerebral inoculation, 4-week-old female ICR mice were purchased from CLEA Japan. Twenty microlitres of 10 % brain homogenate from mice infected with the Obihiro or Chandler strain was injected into the left hemisphere. Twelve-week-old female ICR mice were used to determine the distribution of mAbs and to analyse neuronal toxicity by anti-PrP mAbs.

Intraventricular infusion of mAbs using an osmotic pump. Alzet Mini-Osmotic Pumps, models 2001, 2002 and 2004 (DURECT), were used in this study. Filling of the osmotic pumps with antibody solution was carried out according to the manufacturer's instructions. The pre-filled pumps were then placed in PBS at 37 °C for 24 h. Mice were fitted with a stainless steel cannula supplied with the Alzet Brain Infusion kit (DURECT) and positioned according to stereotaxic coordinates into the left lateral ventricle of the brain (bregma – caudal 1.0 mm, lateral 1.0 mm with a depth of 3 mm below the dura). The osmotic pumps were subsequently implanted subcutaneously into the back and connected to the fitted cannula. All surgical procedures were performed under anaesthesia by intramuscular injection of xylazine (10 mg kg^{-1}) and ketamine (50 mg kg^{-1}). After surgery, cefotaxime (Chugai) was administered subcutaneously (40 mg kg^{-1}) and a gentamicin ointment (Schering-Plough) was pasted on the suture line for 3 days. All mice were housed individually during post-surgery observation periods. Mice that died within a few days of the operation were excluded from the statistical analysis.

Stereotaxic injection of mAbs. Mice were anaesthetized as described above and placed onto a stereotaxic apparatus (Narishige). A linear scalp incision was made and the skull was exposed. Bilateral burr holes were drilled to accommodate stereotaxic placement into the left and right hippocampus (bregma – caudal 2.0 mm, lateral 2.1 mm). Using a Hamilton syringe with a 31-gauge needle, 2 µl mAbs (2 mg ml^{-1}) were injected into the left and right hippocampus, respectively, at a depth of 2 mm below the dura. Injection was carried out over a period of 15 min.

Western blotting. Brains were sagittally hemi-sectioned and homogenized in 10 % (w/v) TMS buffer [50 mM Tris/HCl (pH 7.5), 5 mM $MgCl_2$, 5 % glucose]. To detect PrP^{Sc}, 200 µl brain homogenate was mixed with an equal volume of a detergent buffer [8 % Zwittergent 3-14, 1 % Sarkosyl, 100 mM NaCl, 50 mM Tris/HCl (pH 7.5)] and treated with collagenase (0.5 mg ml^{-1}) for 15 min at 37 °C. The samples were then digested with proteinase K (PK; Roche)

at 20 μg ml^{-1} for 30 min at 37 °C. After terminating PK activity by adding Pefabloc (Roche) at 2 mM, samples were treated with 40 μg DNase I ml^{-1} for 5 min. A half volume of a mixture of 2-butanol and methanol (5 : 1) was added and the PrP^{Sc} was pelleted by centrifugation at 20 000 *g* for 10 min at 20 °C. The resulting pellet was dissolved in 1 × SDS sample buffer [62.5 mM Tris/HCl (pH 6.8), 5 % glycerol, 3 mM EDTA, 4 % β-mercapthoethanol, 0.04 % bromophenol blue, 5 % SDS, 4 M urea] by boiling for 5 min. SDS-PAGE and Western blotting were carried out as described elsewhere (Uryu *et al.*, 2007)

Histopathology and immunohistochemistry. Mouse brains that had been infused with Alexa Fluor 488-conjugated mAbs were frozen in Tissue-Tek OCT compound (Sakura) and cryosections of 16–20 μm were prepared. The sections were dried and fixed with acetone for 10 min. Sections were mounted with Vectashield containing propidium iodine (PI; Vector Laboratories) and examined with a Nikon C1 laser confocal microscope. The presence of infused mAb was also confirmed by direct detection as follows. The sections were reacted with EnVision$^+$ System-labelled polymer conjugated to horseradish peroxidase (HRP) (Dako) for 45 min at 37 °C and positive signals were detected using Simple Stain 3,3′-diaminobenzidine (DAB) solution (Nichirei). This was followed by counterstaining with Mayer's haematoxylin (Wako).

Dissected mouse brains were fixed in 10 % formalin and embedded in paraffin. Sections (4 μm) were deparaffinized, rehydrated and subjected to haematoxylin and eosin (H&E) staining or immunohistochemistry. Antigen retrieval for immunohistochemistry was performed by hydrolytic autoclaving at 135 °C for 20 min for detection of PrP^{Sc} and at 121 °C for 10 min for GFAP and Iba1 (Furuoka *et al.*, 2005). The sections were treated with 3 % H_2O_2 for 5 min, blocked with 10 % normal goat serum for 30 min and then incubated for 45 min at 37 °C with B103 at a dilution of 1 : 100, anti-GFAP at 1 : 5000 or anti-Iba1 at 1 : 100. After washing with PBS, the sections were reacted with EnVision$^+$ System-labelled polymer–HRP for 45 min at 37 °C. The sections were then rinsed and developed with Simple Stain DAB, followed by counterstaining with Mayer's haematoxylin.

Terminal uridine deoxynucleotidyl transferase dUTP nick end labeling (TUNEL) staining. Neuronal cell death was examined using an *In situ* Cell Death Detection kit (Roche). Four micrometer sections of paraffin-embedded brain tissue were deparaffinized, rehydrated and incubated with 10 μg PK ml^{-1} for 10 min at 37 °C. After washing with PBS, the sections were incubated with labelling mixture containing terminal deoxynucleotidyl transferase and digoxigenin-labelled dUTP-conjugated FITC for 60 min at 37 °C. The sections were counterstained with PI and examined with a C1 laser confocal microscope.

RESULTS

Distribution of mAb in brain following intraventricular infusion

We first examined the distribution of mAb infused into the left lateral ventricle of mouse brain. Alexa Fluor 488-conjugated mAb 31C6 (anti-PrP mAb) or P2-284 (negative-control mAb) was infused into the left lateral ventricle and the distribution of mAb was examined at 7, 14, 24 and 34 days after the initiation of infusion. To examine the distribution of the mAbs, brain cryosections at the levels indicated in Fig. 1(a) were prepared. Fig. 1(c) shows the detection of Alexa Fluor 488-conjugated mAb 31C6 in the hippocampus. Fluorescence was detected over the hippocampus (up to 14 days). Although the area of distribution gradually narrowed thereafter, mAbs were still detectable in the hippocampus at 20 days after the termination of infusion (i.e. at 34 days). In contrast, a very low-level fluorescent signal was detected in the hippocampus of a mouse infused with Alexa Fluor 488-conjugated mAb P2-284, even at 7 days after the initiation of infusion. These results suggested that the longer duration of mAb 31C6 in the hippocampus compared with the control mAb was due to binding of mAb 31C6 to PrP^{C}.

Fig. 1(d) summarizes the distribution of the anti-PrP mAb. The mAb was well distributed to areas surrounding the lateral and dorsal third ventricles, hippocampus and thalamus. The mAb was also detected in areas close to the ventral third ventricles. In addition, mAb was detected in regions of the medulla oblongata that face the fourth ventricle and the subarachnoid space, suggesting that the mAb infused into the lateral ventricle was distributed to many parts of brain, presumably via the flow of cerebrospinal fluid. Although the mAb was distributed to parts of the brain parenchyma, distribution of mAb into the cortex and cerebellum appeared to be less efficient. When observing sections under a microscope, we noticed that the mAb-infused hemisphere showed higher fluorescence intensity than that observed in the contralateral side (data not shown), suggesting that the distribution of mAb was not symmetrical. This tendency was confirmed by direct detection of Alexa Fluor 488-conjugated mAb 31C6 (Fig. 1b).

Effects of anti-PrP mAbs on PrP^{Sc} accumulation in the brain

Mice inoculated with Obihiro or Chandler strain reach the terminal stage of the disease at around 150 days post-inoculation (p.i.). Early clinical signs such as ataxia of hind limbs and changes in pelage and posture appear at around 120 days p.i. To evaluate the therapeutic potential of anti-PrP mAbs in a late stage of the disease, infusion of mAbs was started at 120 days p.i. and accumulation of PrP^{Sc} and neurohistopathological lesions were analysed.

Fig. 2(a) shows PrP^{Sc} accumulation in the brains of mice infected with the Obihiro strain at 30 days post-infusion (150 days p.i.). The mean PrP^{Sc} levels in mice treated with mAbs 110, 31C6 and 44B1 were 78, 69 and 77 %, respectively, compared with the control (mAb P2-284; n=2). To determine whether the relative reduction in PrP^{Sc} levels was caused by acceleration of PrP^{Sc} degradation or deceleration of PrP^{Sc} accumulation, we analysed the kinetics of PrP^{Sc} accumulation during the period from 127 to 150 days p.i. (Fig. 2b). There was no difference in PrP^{Sc} levels in mice treated with anti-PrP mAbs compared with those treated with the negative-control mAb at 127 days p.i. (7 days after the initiation of infusion). However, PrP^{Sc} levels increased 2.3-fold in mice treated with the control

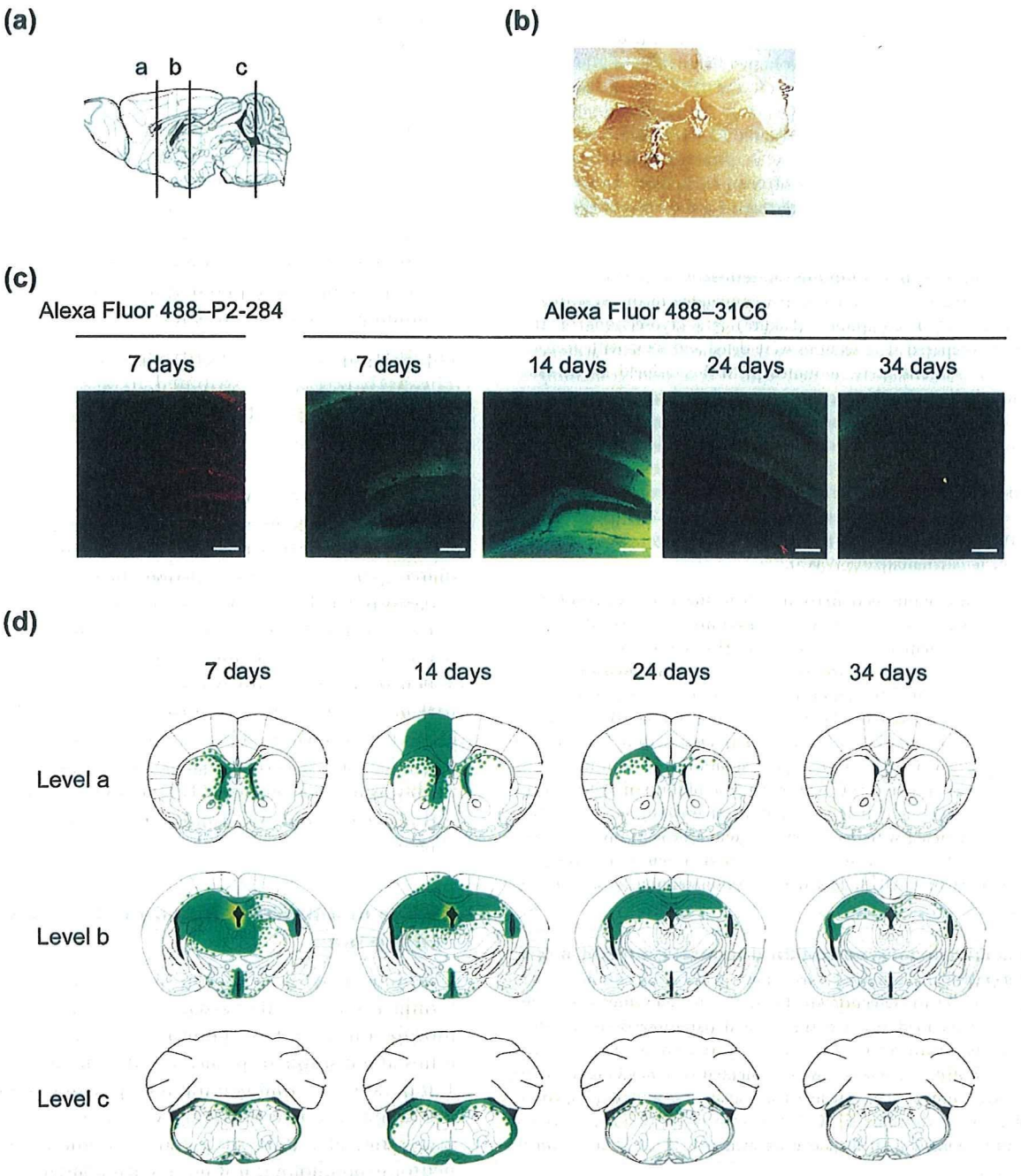

Fig. 1. Distribution of mAbs following intraventricular infusion. Alexa Fluor 488-conjugated mAb 31C6 or P2-284 was infused into the left lateral ventricle using an Alzet Mini-Osmotic Pump model 2002 (mAb concentration 0.5 mg ml^{-1}, pumping rate 0.5 µl h^{-1}, duration 14 days, volume 200 µl). (a) Levels of coronal section examined. Cryosections at the indicated levels were prepared. (b) Detection of mAbs by direct staining. A frozen section at level b was prepared from the brain of a mouse sacrificed at 5 days after starting infusion and the distribution of mAb was visualized by direct staining. Bar, 500 µm. (c) Detection of mAbs in the hippocampus. mAbs conjugated with Alexa Fluor 488 were analysed by laser confocal microscopy. Bars, 200 µm. (d) Distribution of mAb after infusion. The distribution of mAb at 7, 14, 24 and 34 days after starting infusion (green) was superimposed on the images taken from Paxinos & Franklin (2001).

mAb over the period 127–150 days p.i., whereas PrP^{Sc} levels increased only 1.6-, 1.3- and 1.3-fold in mice treated with mAbs 110, 31C6 and 44B1, respectively. These results indicated that anti-PrP mAbs can reduce the rate of PrP^{Sc} accumulation in the brain, even when treatment is initiated at a late stage of the disease.

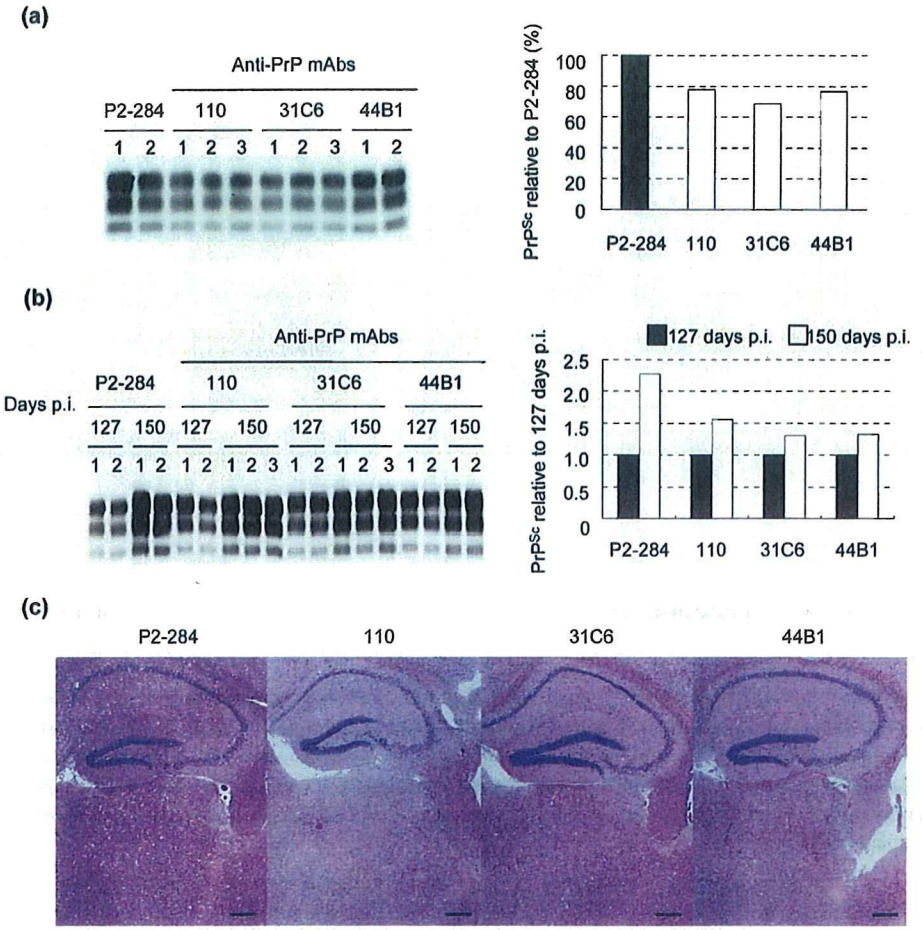

Fig. 2. Effects of anti-PrP mAbs on PrP^{Sc} accumulation and spongiform changes in mice infected with the Obihiro strain. mAbs were infused into the left lateral ventricle of mice inoculated with the Obihiro strain at 120 days p.i. using an Alzet Mini-Osmotic Pump model 2004 (mAb concentration 2 mg ml^{-1}, pumping rate 0.25 µl h^{-1}, duration 28 days, volume 200 µl). Mouse brains were cut sagittally along the midline. The left hemisphere (mAb-infused side) was used for the detection of PrP^{Sc} by Western blotting, whereas the right hemisphere (non-infused side) was fixed with 10 % formalin for paraffin sections. (a) Accumulation of PrP^{Sc} at 150 days p.i. Samples from individual mice (50 µg brain equivalent) were loaded in each lane and the intensities of PrP^{Sc} bands were quantified. The mean intensity for mice treated with the negative-control mAb (P2-284) was designated 100 % and the graph shows relative PrP^{Sc} levels for mice treated with anti-PrP mAbs. (b) Kinetics of PrP^{Sc} accumulation. Mice were sacrificed at 127 and 150 days p.i. and the left hemisphere (mAb-infused side) was used for Western blotting. Samples from individual mice (50 µg brain equivalent) were loaded in each lane and chemiluminescence intensities were quantified. The graph on the right shows the mean level of PrP^{Sc} at 150 days p.i. compared with the level at 127 days p.i. Samples at 150 days p.i. were the same as those in (a). (c) Spongiform changes at 150 days p.i. Paraffin sections were prepared from the contralateral hemisphere of the brain described in (a) and stained with H&E.

Effects of anti-PrP mAbs on neurodegeneration

Next, we investigated the effects of mAbs on neurodegeneration. To do this, the contralateral hemispheres of brains used in Fig. 2(a) (at 150 days p.i.) were examined histopathologically. Although mAbs were more readily detected in the infused side than in the contralateral side (Fig. 1), spongiform changes in the hippocampus and thalamus of mice treated with mAbs 110, 31C6 and 44B1 were nevertheless milder than those treated with the negative-control mAb (Fig. 2c).

Immunohistochemical examination also revealed that anti-PrP mAbs affected the progression of neuropathological lesions in mice infected with the Obihiro strain (Fig. 3). Consistent with the reduction in PrP^{Sc} levels by anti-PrP mAbs (Fig. 2a), PrP^{Sc} deposition in the hippocampus and thalamus of mice infused with mAbs 110 and 31C6 was milder than in the negative control. In addition, astrogliosis (as evaluated by GFAP staining) appeared to be reduced in mice treated with anti-PrP mAbs compared with the negative control. Microglial activation in the

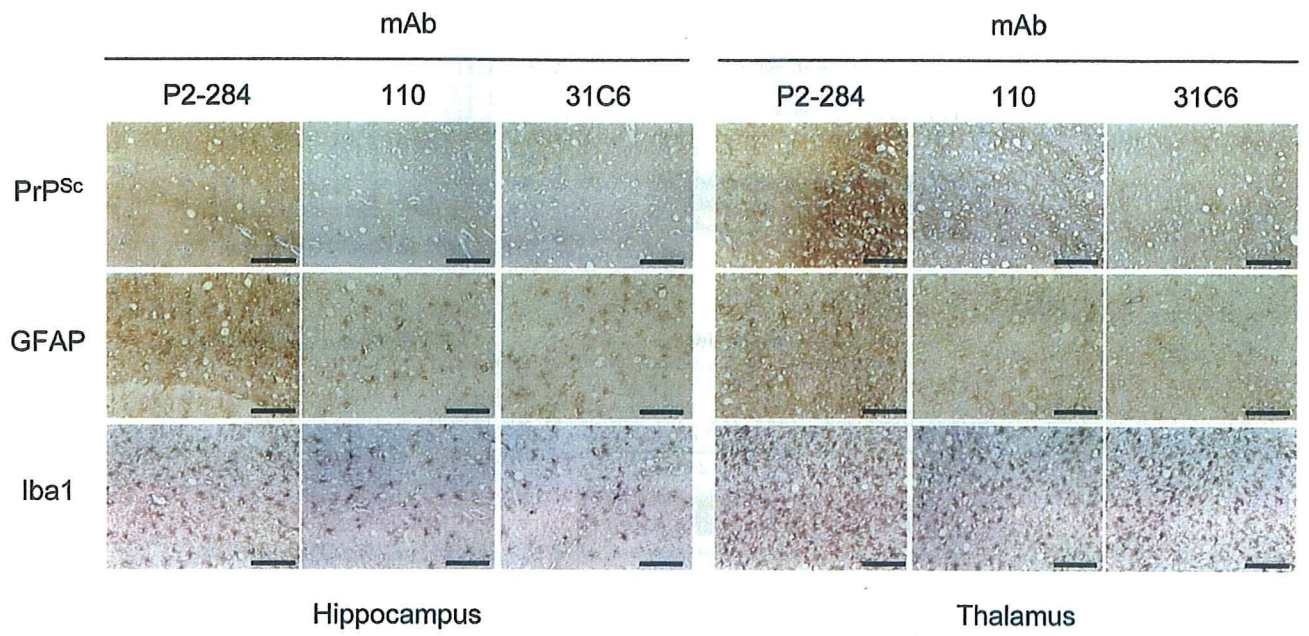

Fig. 3. Effects of anti-PrP mAbs on PrP^{Sc} accumulation and gliosis in mice infected with the Obihiro strain. Intraventricular infusion of mAbs was carried out as described in Fig. 2 and brains collected at 150 days p.i. were used for analysis. The mice shown in this figure belonged to an independent experimental group (i.e. different from the experimental group shown in Fig. 2). Paraffin-embedded sections were stained with B103 antibodies to detect PrP^{Sc}, anti-GFAP antibodies to detect astrocytes and anti-Iba1 antibodies to detect microglia. Images of the hippocampus and thalamus are indicated. All images represent the mAb-infused side. Bars, 200 μm.

hippocampus (as detected with anti-Iba1 antibodies) was also reduced in the presence of anti-PrP mAbs; in contrast, the effect was marginal in the thalamus.

To investigate the effects of anti-PrP mAbs on different prion strains, we carried out the same experiment using mice infected with the Chandler strain. Similar to what was observed for mice infected with the Obihiro strain, in mice infected with the Chandler strain, mAb 31C6 reduced spongiform changes and PrP^{Sc} deposition in the hippocampus and thalamus compared with the negative-control mAb (Fig. 4). However, the effect of anti-PrP mAb on gliosis appeared to differ for the two different prion strains. Anti-PrP mAbs apparently reduced astrogliosis in the hippocampus and thalamus of mice infected with the Obihiro strain (Fig. 3), but only a slight reduction in astrogliosis was observed for mice infected with the Chandler strain (Fig. 4). Moreover, although microglial activation in the thalamus of mice infected with the Obihiro strain was slightly reduced by treatment with anti-PrP mAbs, it was obviously reduced relative to controls by treatment with mAb 31C6 in mice infected with the Chandler strain (Fig. 4). However, microglial activation as a whole appeared to be moderate in mice infected with the Chandler strain compared with the Obihiro strain; thus, the difference observed could be due to a difference in the level of activation of the microglia between mice infected with the two prion strains.

Prolongation of survival time

To determine whether treatment with anti-PrP mAbs can prolong survival of prion-infected mice when administered at different stages in progression of the disease, infusion was started at a middle stage of infection (60 or 90 days p.i.) and after clinical onset (120 days p.i.). In mice infected with the Obihiro strain, infusion of mAb 31C6 initiated at 60 days p.i. prolonged survival by about 11 days compared with the negative control; however, no effect was observed when infusions were initiated at 90 or 120 days p.i. (Fig. 5 and Table 1). In contrast, for mice infected with the Chandler strain, prolongation of survival was observed in all three groups: infusion initiated at 60, 90 or 120 days p.i. prolonged survival by approximately 10, 13 or 12 days, respectively. Brain sections (H&E stained) of all mice were examined for possible causes of death other than prion disease. Of 96 mice tested, two had severe abscesses around the infused area and thus were excluded from the experimental group.

Changes in body weight were consistent with prolonged survival times. For experimental groups in which survival was prolonged by infusion with mAb 31C6, the decrease in body weight observed in control groups was delayed by about 1 or 2 weeks (Fig. 6). In contrast, no difference was observed for mice infected with the Obihiro strain when mAb infusion was started at 90 or 120 days p.i.

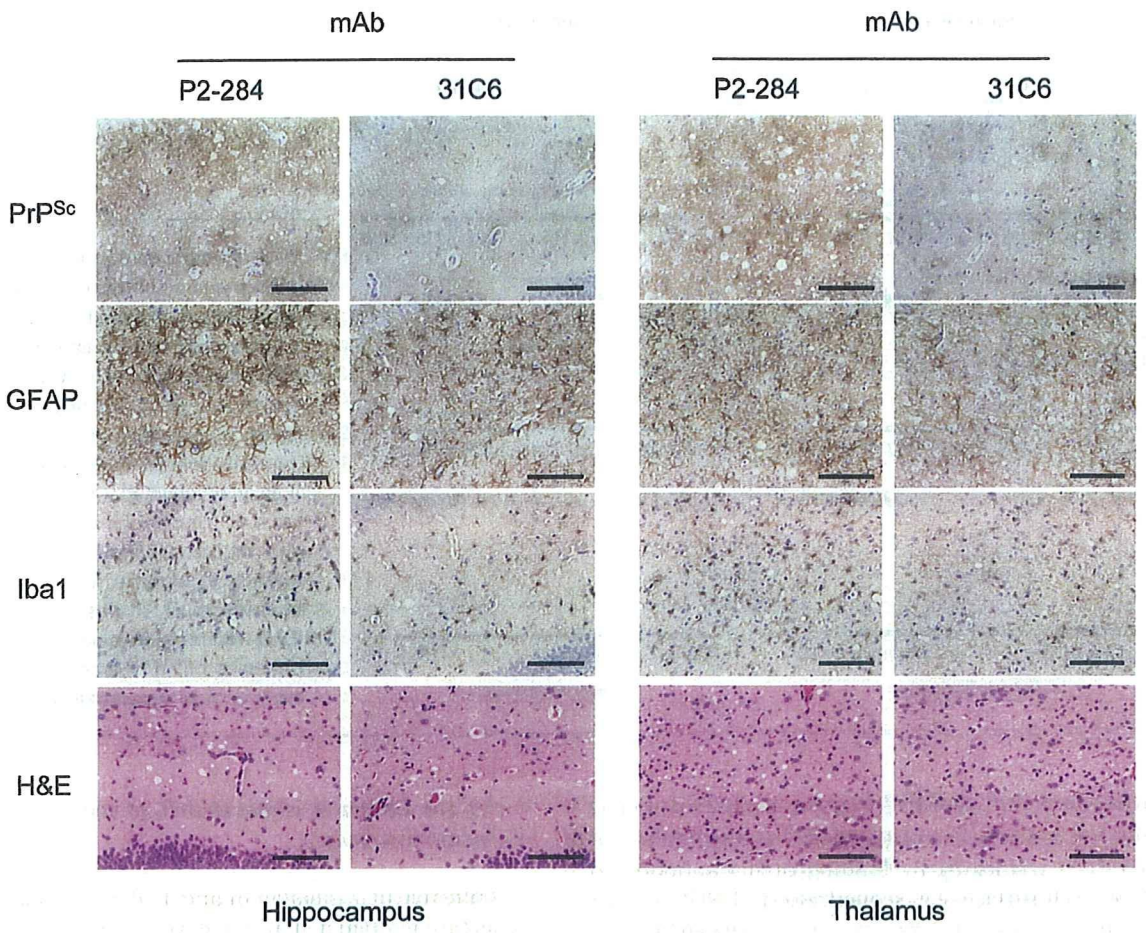

Fig. 4. Effects of anti-PrP mAbs on neuropathological changes in mice infected with the Chandler strain. Intraventricular infusion of mAbs was carried out as described in Fig. 2 using mice inoculated with the Chandler strain and brains collected at 150 days p.i. were used for analysis. The hippocampus and thalamus from mAb-infused hemispheres are shown. Bars, 100 μm.

Neuronal toxicity of mAbs

As it has been reported that an anti-PrP mAb recognizing aa 95–105 of murine PrP can induce apoptosis in hippocampal neurons (Solforosi *et al.*, 2004), we assessed the neurotoxicity of the mAbs used in this study. First, mAbs were infused into the lateral ventricle for 7 days using an Alzet Mini-Osmotic Pump model 2001 (mAb concentration 1 mg ml^{-1}, pumping rate 1 μl h^{-1}, duration 7 days, volume 200 μl); however, no difference was observed between mice treated with anti-PrP mAbs and those treated with the negative-control mAb (data not shown). To assess neurotoxicity directly, we next stereotaxically injected anti-PrP mAbs and the control mAb into the left and right hippocampus, respectively. The distribution of mAb in the hippocampus was confirmed by injecting Alexa Fluor 488-conjugated mAb 31C6 (Fig. 7a). Although mAb was well-distributed throughout the entire hippocampus on the injected side, TUNEL-positive cells were only detected in a limited area of the pyramidal layer and this was observed even in the right side (the side injected with the control mAb P2-284). Indeed, the TUNEL-positive cells were close to the injection site, suggesting that the TUNEL-positive cells resulted from the trauma of mAb injection. It was interesting that mAbs 106 and 110 recognizing the region adjacent to aa 95–105 did not induce apparent neuronal death.

DISCUSSION

In this study, we investigated the effects of anti-PrP mAbs on progression of prion disease, focusing on treatment during late stages of infection. We showed that anti-PrP mAbs antagonized PrP^{Sc} formation in the brain when intraventricular administration was initiated at the time of clinical onset (Figs 2 and 3). The effect of anti-PrP mAbs appeared to be mainly due to deceleration of PrP^{Sc} formation rather than active degradation of PrP^{Sc}. Several reports have suggested that binding of anti-PrP antibodies to the first α-helical domain of PrP^{C} (aa 143–155), which is proposed to be important for the PrP^{C}–PrP^{Sc} interaction (Morrissey & Shakhnovich, 1999; Speare *et al.*, 2003), prevents PrP^{Sc} formation by inhibiting the direct inter-

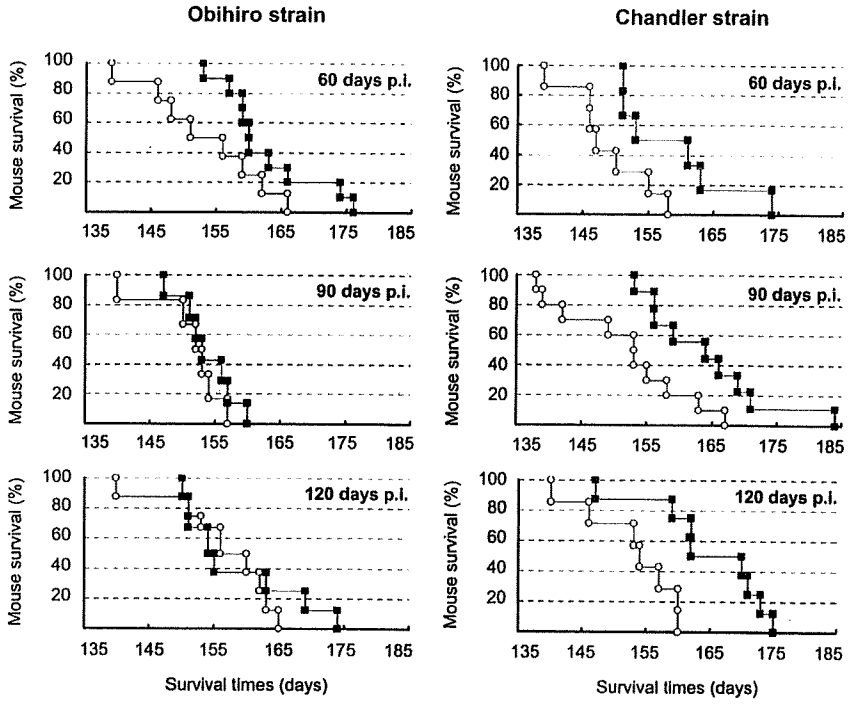

Fig. 5. Intraventricular infusion of anti-PrP mAb prolongs survival. Intraventricular infusion of mAbs into mice inoculated with the Obihiro or Chandler strain was initiated at 60, 90 or 120 days p.i. using an Alzet Mini-Osmotic Pump model 2002 (antibody concentration 2 mg ml^{-1}, pumping rate 0.5 µl h^{-1}, duration 14 days, volume 200 µl). Mice were observed until they reached the terminal stage of the disease. The graphs show survival curves, and survival times (means ± SD) in days are shown in Table 1, together with the numbers of mice in each group. ○, Mice treated with mAb P2-284; ■, mice treated with mAb 31C6. The presence of PrP^{Sc} was confirmed by Western blotting in all experimental-group mice.

action between PrP^{C} and PrP^{Sc} (Enari *et al.*, 2001; Peretz *et al.*, 2001). It has also been suggested that a perturbation of the usual PrP^{C} trafficking by binding of the antibody to PrP^{C} on the cell surface, e.g. sequestration of PrP^{C} on the cell membrane, may be one of the mechanisms of inhibition (Kim *et al.*, 2004b; Feraudet *et al.*, 2005). Consistent with our previous observations (Kim *et al.*, 2004b), mAbs directed against the C-terminal domain (mAb 44B1) and the octapeptide repeat in the N-terminal region (mAb 110), as well as one directed against the first α-helix (mAb 31C6), antagonized PrP^{Sc} formation in the mouse brain (Fig. 2). Indeed, anti-PrP mAb infused into the lateral ventricle was still detectable in the hippocampus at 20 days after the termination of infusion, whereas only a low level of the negative-control mAb was detected in the same region, even during infusion (Fig. 1). These results suggest that the antibody–PrP^{C} complex remains in the brain parenchyma and therefore that sequestration of PrP^{C} by the antibody is implicated in the inhibition of PrP^{Sc} formation *in vivo*.

Intraventricular infusion of anti-PrP mAbs at a late stage of infection (initiated at 120 days p.i.) reduced levels not only of PrP^{Sc} accumulation but also of microglial activation, astrogliosis and spongiform changes. Comparison of neurohistopathological changes observed at 127 versus 150 days p.i. in mice treated with anti-PrP mAbs and the negative-control mAb revealed an apparent reduction in gliosis observed at 150 days p.i., which may be due to a slowdown in the progression of gliosis (data not shown). Although the severity of microglial activation and astrogliosis differed in animals infected with the two different prion strains, the reduction observed was in accordance with the mAb distribution, and the levels of microglial activation and astrogliosis in the hippocampus and thalamus of mice infused with anti-PrP mAbs appeared

Table 1. Effect of intraventricular infusion of anti-PrP mAbs on survival of mice infected with the Obihiro or Chandler strain

Initiation of mAb infusion (days p.i.)	Survival time of mice [mean ± SD (days)]			
	Obihiro strain		Chandler strain	
	P2-284 (*n*)	31C6 (*n*)	P2-284 (*n*)	31C6 (*n*)
60	153.4 ± 9.0 (8)	163.5 ± 8.1* (10)	150.7 ± 10.2 (7)	161.0 ± 8.3* (6)
90	152.8 ± 4.3 (6)	153.3 ± 3.5 (7)	151.7 ± 9.8 (10)	165.0 ± 10.9* (9)
120	154.4 ± 9.4 (8)	157.4 ± 7.0 (8)	152.9 ± 7.4 (7)	164.9 ± 9.3* (8)

*Statistically significant difference based on Student's *t*-test ($P<0.05$).